

Spiers Memorial Lecture: Coordination networks that switch between nonporous and porous structures: an emerging class of soft porous crystals

Shi-Qiang Wang, ^a Soumya Mukherjee ^{ab}
and Michael J. Zaworotko  ^{*a}

Received 1st June 2021, Accepted 14th June 2021

DOI: 10.1039/d1fd00037c

Coordination networks (CNs) are a class of (usually) crystalline solids typically comprised of metal ions or cluster nodes linked into 2 or 3 dimensions by organic and/or inorganic linker ligands. Whereas CNs tend to exhibit rigid structures and permanent porosity as exemplified by most metal-organic frameworks, MOFs, there exists a small but growing class of CNs that can undergo extreme, reversible structural transformation(s) when exposed to gases, vapours or liquids. These "soft" or "stimuli-responsive" CNs were introduced two decades ago and are attracting increasing attention thanks to two features: the amenability of CNs to design from first principles, thereby enabling crystal engineering of families of related CNs; and the potential utility of soft CNs for adsorptive storage and separation. A small but growing subset of soft CNs exhibit reversible phase transformations between nonporous (closed) and porous (open) structures. These "switching CNs" are distinguished by stepped sorption isotherms coincident with phase transformation and, perhaps counterintuitively, they can exhibit benchmark properties with respect to working capacity (storage) and selectivity (separation). This review addresses fundamental and applied aspects of switching CNs through surveying their sorption properties, analysing the structural transformations that enable switching, discussing structure-function relationships and presenting design principles for crystal engineering of the next generation of switching CNs.

1. Introduction

Coordination networks (CNs)¹ are a class of covalent network solids comprised of metal or metal clusters (nodes) connected in two or more directions by organic (e.g. metal-organic frameworks, MOFs^{2,3}), inorganic (e.g. Prussian blue and its

^aBernal Institute, Department of Chemical Sciences, University of Limerick, Limerick V94 T9PX, Republic of Ireland. E-mail: Michael.Zaworotko@ul.ie

^bDepartment of Chemistry, Technical University of Munich, Lichtenbergstraße 4, 85748 Garching bei München, Germany



analogues, PBAs^{4,5}) or combinations of organic and inorganic (*e.g.* hybrid ultramicroporous materials, HUMs⁶) linker ligands (Fig. 1). CNs are a subset of coordination polymers (CPs)^{7,8} and represent an extraordinarily diverse and growing class of metal–organic materials (MOMs).^{9,10} Interest in CNs is at least partly due to their inherent modularity and amenability to crystal engineering or reticular chemistry,^{11,12} which in turn facilitates the generation of closely related families of materials that allow for systematic structure–function studies. One property in particular has attracted the attention of researchers, namely porosity. Porosity is a direct outcome of the “node-and-linker” approach to the design of CNs that can be credited to Robson and Hoskins, who introduced the concept as a design principle for the generation of porous solids over 30 years ago.^{13,14} The existence of porosity deservedly attracts attention but is not in itself the only thing that makes CNs of special interest. Rather, it is the inherent modularity of CNs that brings with it an ability to design pore size, shape and chemistry. This in turn enables fine-tuning of properties to create potential utility for new energy-efficient technologies in areas of societal need, *e.g.* gas/vapour storage, separations, water purification, drug delivery and catalysis.^{15–19} Thus far, around 100 000 CNs have been deposited in the MOF subset of the Cambridge Structural Database (CSD),²⁰ thereby accounting for *ca.* 10% of entries in the CSD.²¹ The majority, perhaps >99%, of CNs thus far reported can be classified as “first generation” or “second generation” CPs,^{7,22–24} which either undergo structural collapse (first generation) or possess rigid structures like zeolites (second generation) upon guest removal, respectively. Herein, we address a small subset of “third generation” or “soft” CPs that are stimulus responsive in that they change structure when exposed to gases, vapours or liquids.

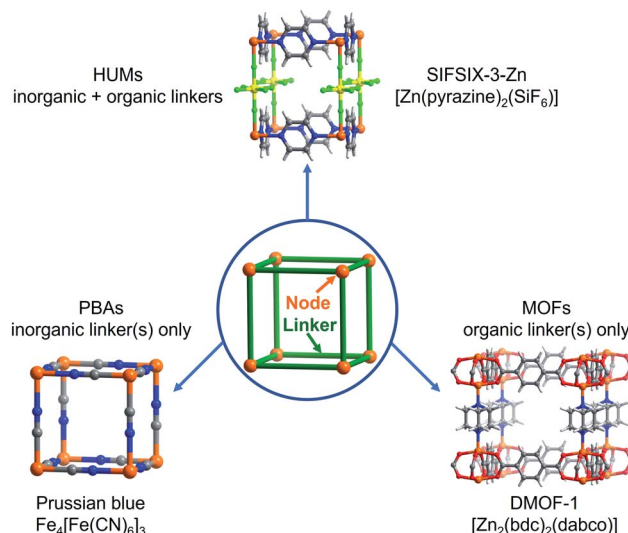


Fig. 1 CNs can be classified into three subsets by the type of linker ligands: inorganic only (*e.g.* PBAs); organic only (*e.g.* MOFs); hybrid (*e.g.* HUMs). The three subsets are exemplified by Prussian blue, DMOF-1 and SIFSIX-3-Zn, respectively.



Seminal discoveries in the late 1990s and early 2000s²⁵⁻²⁹ introduced “third generation” CPs^{7,22-24} or “soft porous crystals”.^{30,31} Third generation CNs exhibit structural flexibility when exposed to external stimuli such as light,³² heat,³³ mechanical pressure³⁴ and/or guest molecules.³⁵⁻³⁷ Pioneered by Kitagawa, Férey and others,^{7,22-24,38-41} flexible CNs have been comprehensively reviewed from different perspectives such as smart switches^{42,43} multiscale design,⁴⁴ *in situ* characterisation,⁴⁵ controlled flexibility design,⁴⁶ simulation and computational studies⁴⁷ and overall progress.⁴⁸⁻⁵⁰ Herein we focus upon a small but growing and potentially important subset of flexible CNs, namely those 2D (*e.g.* ELM-11 (ref. 28)) and 3D (*e.g.* $[\text{Cu}_2(\text{bdc})_2(\text{bpy})]^{51}$) CNs that switch between closed (nonporous) and open (porous) phases.

A variety of terms have been coined to describe the flexibility of CNs including “accordionlike”,²⁶ “springlike”,^{27,52} “spongelike”,^{53,54} “breathing”,⁵⁵ “swelling”,^{56,57} “soft”,^{30,31,58} “elastic”,^{59,60} “dynamic”,^{24,61,62} “stimuli-responsive”,^{47,63,64} and “gate-opening”.^{28,65,66} An alternate approach to classify flexible CNs is to use their sorption isotherms and we have proposed a classification system based upon sorption isotherm types, namely type F-I to type F-V.⁶⁷ IUPAC has classified type I isotherms as being characteristic of rigid microporous adsorbents thanks to the enhanced adsorbent-adsorbate interactions which results in micropore filling at very low relative pressure (Fig. 2a).⁶⁸ In contrast, flexible microporous CNs usually exhibit distinct “stepped” or “S-shaped” isotherm profiles that are yet to be

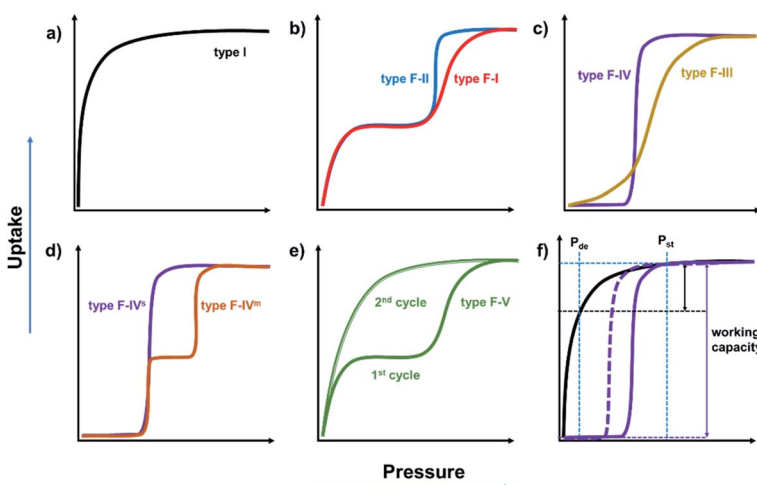


Fig. 2 Schematic illustration of sorption isotherm types exhibited by CNs. (a) Type I, typical of rigid microporous CNs; (b) type F-I (open to more open, gradual) and F-II (open to more open, sudden), associated with flexible microporous CNs; (c) type F-III (closed to open, gradual) and F-IV (closed to open, sudden) associated with switching nonporous CNs; (d) type F-IV isotherms can be sub-divided into single-step type F-IV^s and multiple-step (≥ 2) type F-IV^m isotherms; (e) type F-V isotherms are indicative of a shape memory effect in second and subsequent consecutive sorption cycles; (f) comparison of working capacity between type I and F-IV isotherms with similar surface areas: black line = adsorption branch of type I isotherm (desorption branch overlays); solid/dash purple lines = adsorption and desorption branches of type F-IV isotherm, respectively; P_{de} : delivery pressure; P_{st} : storage pressure.



formally classified by IUPAC. When flexible CNs retain porosity after activation, a type I-like profile will be followed by the second step at a threshold pressure that coincides with a structural transformation from a less open phase to a more open phase. This transformation could be gradual (type F-I, *e.g.* the “breathing” effect in MIL-53(Cr)⁶⁹) or sudden (type F-II, *e.g.* the “gate-opening” effect in ELM-12 (ref. 70)) (Fig. 2b). When flexible CNs are nonporous after activation, the transformation from a nonporous (closed) to a porous (open) phase can also occur gradually (type F-III, *e.g.* the “swelling” effect in $[\text{Co}_2(\text{BME-bdc})_2(\text{dabco})]^{\text{71}}$) or suddenly (type F-IV, *e.g.* the “switching” effect in $[\text{Zn}_2(\text{BME-bdc})_2(\text{dabco})]^{\text{71}}$) (Fig. 2c). In addition, type F-IV isotherms can be further sub-divided depending on the number of sorption steps, *i.e.*, single-step type F-IV^s or multiple-step (≥ 2) type F-IV^m (Fig. 2d).⁷² We note that most of the flexible CNs reported to date undergo reversible structural changes in response to the presence/absence of external stimuli and that there are very few examples of flexible CNs that do not return to their activated forms after full desorption. There are, however, CNs that retain the structure of the fully open stage after the first sorption cycle and exhibit type I sorption isotherms during the subsequent cycles (type F-V, *e.g.* the “shape memory” effect in X-pcu-3-Zn-3i⁷³) (Fig. 2e). Amongst the various isotherm types in Fig. 2, flexible CNs that exhibit type F-IV isotherms are perhaps the most desirable with respect to gas storage as they can offer higher working capacity than rigid porous materials with type I isotherms (Fig. 2f).^{72,74} It should be mentioned that hysteresis is a feature of most type F-IV isotherms and, to be of practical utility, the delivery pressure (P_{de}) must be lower than the desorption branch rather than the adsorption branch (Fig. 2f).

We adopt the term “switching” herein as it is consistent with the “on/off” nature of CNs that exhibit reversible “closed/open” structural changes of the type that affords type F-IV isotherms. Switching has also been used for other on/off events in materials chemistry such as thermal expansion/shrinkage, spin crossover, redox, photochromism, photoisomerization and valence tautomerism.^{42,43,75-77} In the following sections, we analyse and discuss reversible switching in the context of guest sorption by presenting case studies of switching CNs with particular emphasis upon structure–property relationships and the influence of variables such as metal node, linker ligand, and adsorbate.

2. Switching CNs

Whereas coordination complexes and organic molecules are long-known for the ability to exhibit guest inclusion or clathration that accompanies switching between closed and open phases,⁷⁸⁻⁸³ the first examples of 2D and 3D switching CNs were not reported until the beginning of the 21st century (Fig. 3).^{28,51} Werner complexes are prototypal coordination compounds and their guest-clathration ability was systematically studied by Schaeffer in 1957.⁷⁸ The associated sorption isotherms were reported in 1969 by Barrer’s group, who studied the sorption behaviour of several Werner complexes upon exposure to a range of gases and vapours.⁷⁹ Type F-IV isotherms were observed when the Werner complex $[\text{Co}(\text{etyl})_4(\text{NCS})_2]$ was exposed to benzene, toluene and xylenes and this phenomenon was attributed to closed/open phase transformations. We recently reported a related example of such a Werner complex and termed it as a Switching Adsorbent Molecular Material (SAMM).⁸³ The first 2D switching CN,



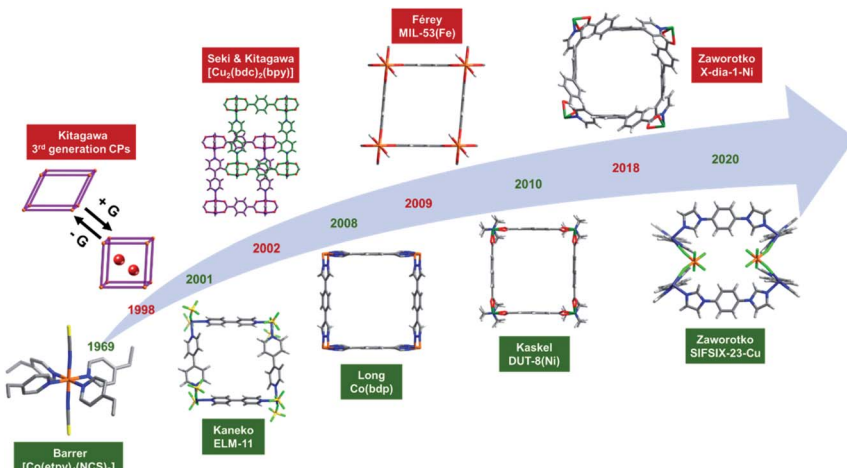


Fig. 3 Chronology of key developments related to switching CNs. 1969 (Barrer): type F-IV^s sorption isotherms observed in the Werner complex $[\text{Co}(\text{etylpyridine})_4(\text{NCS})_2]$; 1998 (Kitagawa): 3rd generation CPs defined; 2001 (Kaneko): first 2D switching CN, ELM-11, reported; 2002 (Seki & Kitagawa): first 3D switching and “shape-memory” CN, $[\text{Cu}_2(\text{bdc})_2(\text{bpy})]$, detailed; 2008 (Long): type F-IV^m sorption isotherms observed in $\text{Co}(\text{bdp})$, currently the benchmark switching CN for CH_4 storage; 2009 (Férey): reported the most widely studied switching CN: MIL-53(Fe); 2010 (Kaskel): benchmark N_2 (77 K) and CO_2 (195 K) uptakes for DUT-8(Ni); 2018 (Zaworotko): first **dia** topology switching CN, X-dia-1-Ni, and classification of the isotherm types for flexible CNs; 2020 (Zaworotko): first example of switching hybrid CN with inorganic and organic linkers, SIFSIX-23-Cu, published.

$[\text{Cu}(\text{bpy})_2(\text{BF}_4)_2]$, ELM-11,²⁸ was reported in 2001 and can be regarded as being comprised of linked Werner complexes which serve as molecular building blocks (MBBs⁸⁴). The first 3D switching CN, $[\text{Cu}_2(\text{bdc})_2(\text{bpy})]$,⁵¹ was reported in 2002 and features a 2D square lattice layer comprised of linked “paddle-wheel” MBBs that is pillared by bpy linkers to form a 2-fold interpenetrated 3D network. Altering the length of the vertical pillar and horizontal linker afforded a non-interpenetrated switching CN DUT-8(Ni) which set benchmark uptakes for N_2 (77 K) and CO_2 (195 K) in switching CNs.^{113,114} Hybrid CNs⁶ with primitive cubic (**pcu**) topology can be generated from 2D square lattice (**sql**) CNs when an inorganic counter anion such as hexafluorosilicate can serve as a pillar ligand, as exemplified by the first switching hybrid CN, SIFSIX-23-Cu.¹⁵¹ Whereas the coordination spheres of Werner complexes, 2D **sql** CNs and 3D **pcu** CNs are chemically related, their dimensional rigidities can be different.⁴⁰ In 2008, type F-IV^m isotherms were observed in $\text{Co}(\text{bdp})$,¹⁰¹ which later set a benchmark for volumetric CH_4 working capacity in the context of switching CNs.⁷⁴ Although MIL-53 CNs were reported as early as 2002, a switching variant, MIL-53(Fe), was not introduced until 2009.¹⁰⁶ X-dia-1-Ni, reported in 2018, was the first example of a diamondoid (**dia**) topology switching CN and it was found to exhibit the second highest CH_4 working capacity in switching CNs.⁶⁷ Overall, around 60 switching CNs have now been reported (Table 1), with **sql** and **pcu** topology CNs being the most common 2D and 3D switching CNs, respectively. Whereas 2D switching CNs were reported first, the proportion of 3D switching CNs is currently much higher than 2D switching CNs



Table 1 Tabulated chronology (2001–2020) of switching CNs

CNs	Dimension	Guests	Year	Ref.
ELM-11	2D	N ₂ , Ar, O ₂ , CH ₄ , CO ₂ , C ₂ H ₂ , C ₄ H ₁₀	2001	28, 72 and 85–90
[Co(NCS) ₂ (3-pia) ₂]	2D	Me ₂ CO	2002	91
[Cu ₂ (pzdc) ₂ (dpvg)]	3D	MeOH, H ₂ O	2002	92
[Cu ₂ (bdc) ₂ (bpy)]	3D	N ₂ , CH ₄ , MeOH, CO ₂	2002	51 and 93
[Cu(dhbc) ₂ (bpy)]	2D	O ₂ , N ₂ , CH ₄ , CO ₂	2003	65 and 94
[Co(NCS) ₂ (4-peia) ₂]	2D	Me ₂ CO	2004	95
[Cu(pyrdc)(bpp)]	2D	CO ₂ , MeOH, EtOH	2005	96
MOF-508	3D	N ₂ , H ₂ , CO ₂ , C ₂ H ₂	2006	97–99
[Zn(TCNQ) ₂ (bpy)]	3D	C ₆ H ₆	2007	100
[Cd(bpndc)(bpy)]	2D	O ₂ , N ₂ , Ar	2008	66
Co(bdp)/Fe(bdp)	3D	N ₂ , H ₂ , CH ₄ , CO ₂	2008	74 and 101–103
ELM-31	2D	CO ₂	2009	104
SNU-M11/SNU-M10	3D	CO ₂	2009	105
MIL-53(Fe)	3D	CH ₄ , C ₂ H ₆ , C ₃ H ₈ , C ₄ H ₁₀ , CO ₂ , C ₈ H ₁₀	2009	106–108
[Cd ₂ (pzdc) ₂ L]	3D	CO ₂	2009	109
[Zn(pydc)(dma)]	3D	N ₂ , Ar, CO ₂ , H ₂ , CH ₄	2009	110
Zn(GA) ₂	3D	CO ₂	2010	111
CID-5	2D	CO ₂	2010	112
DUT-8(Ni)	3D	CO ₂ , N ₂ , Xe, C ₄ H ₁₀ , C ₂ H ₄ , C ₂ H ₆ , MeCN, C ₇ H ₈ , C ₇ H ₁₆ , CH ₂ Cl ₂ , CHCl ₃ , CCl ₄	2010	113–117
[Zn ₂ (bpdc) ₂ (bpee)]	3D	N ₂ , Ar, CO ₂ , C ₂ H ₂ , C ₂ H ₄ , C ₂ H ₆ , C ₃ H ₆ , C ₃ H ₈ , 2010 118 and C ₄ H ₁₀	2010	119
[Zn ₂ (bdc) ₂ (dfpbp)]	3D	O ₂ , Ar, CO ₂	2011	120
[Zn(DIP-bdc) ₂ (dabco)]	3D	CO ₂	2012	121
[Zn(DB-bdc) ₂ (dabco)]				
MIL-53(Sc)	3D	CO ₂	2012	122 and 123
[Ni(bdc)(bphy)]	2D	CO ₂	2012	124
[Cu(CF ₃ SO ₃) ₂ (bpp)]	2D	O ₂ , CO ₂	2013	125
[Zn ₂ L ₂]	3D	N ₂ , CH ₄	2014	126
DynaMOF-100	3D	C ₈ H ₁₀ , C ₈ H ₈	2014	127 and 128
JLU-Liu3/JLU-Liu4	3D	N ₂	2014	129
[Ag ₂ (L15) ₂]	3D	CO ₂	2014	130
[Sm(HL)(DMA) ₂]	3D	CO ₂ , CH ₂ Cl ₂	2015	131
f-MOF-1/f-MOF-2	3D	CO ₂	2016	132
Co(F ₂ -bdp)/Co(Me ₂ -bdp)	3D	N ₂ , CH ₄	2016	133
Mn(ina) ₂	3D	C ₂ H ₆ , C ₃ H ₆ , C ₃ H ₈	2016	134
JLU-Liu33	3D	N ₂	2017	135
[Zn ₂ (DPT) ₂ (bpy)]	3D	CO ₂	2017	136
[Zn ₃ (bdc) ₂ (tz) ₂]	3D	C ₂ H ₆ , C ₃ H ₈ , C ₄ H ₁₀	2017	137
[Co(VTTF)]	2D	C ₂ H ₄	2017	138
DUT-98	3D	N ₂ , H ₂ O	2017	139 and 140
CPM-325	3D	N ₂ , CO ₂	2018	141
Cd(miba) ₂	3D	CO ₂	2018	142
[Zn ₂ (tdc) ₂ (pvq)]	3D	N ₂	2018	143



Table 1 (Contd.)

CNs	Dimension	Guests	Year	Ref.
Zn ₂ (BME-bdc) ₂ (dabco)	3D	CO ₂	2018	71
X-dia-1-Ni	3D	CO ₂ , CH ₄	2018	67
sql-1-Co-NCS	2D	CO ₂ , C ₈ H ₁₀	2018	144 and 145
X-pcu- <i>n</i> -Zn, <i>n</i> = 5, 6, 7, 8	3D	CO ₂ , C ₂ H ₂	2018	146 and 147
NJU-Bai8	3D	C ₃ H ₆ , C ₃ H ₈	2018	148
[Zn ₂ (ndc) ₂ (bpa)]	3D	CO ₂	2019	149
[Cu(HIsa-az-dmpz)]	3D	N ₂ , CO ₂	2019	150
SIFSIX-23-Cu (NTU-65)	3D	N ₂ , CO ₂ , C ₂ H ₂ , C ₂ H ₄	2020	151 and 152
ELM-13	2D	N ₂ , O ₂ , Ar, NO, CO ₂	2020	153
JUK-8	3D	CO ₂ , H ₂ O	2020	154

(~4 : 1). This is likely a reflection of the larger number of 3D CNs (especially MOFs) that have been studied for their sorption properties in the past two decades but should not imply any prejudice in favour of modularity or properties for 3D CNs *versus* 2D CNs.

Switching between a closed and a single open phase generally results in single-step type F-IV^s isotherms^{51,65,66,71,74} whereas switching between closed and multiple open phases usually affords multiple-step type F-IV^m isotherms (Fig. 2d and 4).^{72,85-87} The number of structural transitions and/or sorption steps in a switching CN can be influenced by factors such as temperature, pressure and adsorbate as exemplified by ELM-11.^{72,85-87} Several of the prototypal switching CNs are modular and amenable to crystal engineering through systematic variation of metal moieties, linker ligands, sorbates or a combination thereof. Importantly, in many published reports, both the closed and open phases are structurally characterized and/or computationally modelled, thereby providing insight into both the mechanism of switching and the nature of the sorbent–sorbate interactions

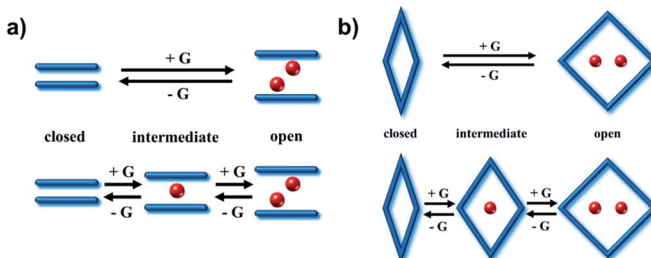


Fig. 4 Schematic illustration of the types of structural transformations in (a) 2D and (b) 3D switching CNs induced by sorbate/guest molecules (G, red balls). Transformation between closed and open phases typically results in a single-step type F-IV^s isotherm (top). Transformation between closed, intermediate (partially open) and fully open phases generally leads to a type F-IV^m isotherm (bottom).



that drive the switching event. In the following sections, we present case studies of representative switching CNs and succinctly analyse their switching behaviour.

2.1. Examples of 3D switching CNs

2.1.1 MIL-53(M) family [M(OH)(bdc)]. The MIL-53 family of CNs represents perhaps the most widely studied family of flexible CNs thanks to the contributions of Férey and others.¹⁵⁵ The metals (M) of MIL-53 are trivalent, *e.g.* Cr, Al, Fe, Sc, Ga or In.^{156–161} The structure of MIL-53(M) CNs is sustained by infinite *trans* corner sharing $[\text{MO}_4(\text{OH})_2]$ octahedra that form 1D chains by serving as rod building blocks, RBBs,^{162–164} which are cross-linked through bdc ligands (bdc = 1,4-benzenedicarboxylate) to afford **sra** topology networks (Fig. 5).¹⁶² The resulting 1D rhombic tunnels are occupied by solvent or guest molecules. The first members of the MIL-53(M) family, MIL-53(Cr) and MIL-53(Al), were reported in 2002 and 2003, respectively.^{156,157} Initial studies focused on structural transformations during hydration–dehydration processes.^{165,166} Large and reversible phase transformation between the activated “open” phase (MIL-53ht, ht = high temperature) and hydrated “contracted” phase (MIL-53lt, lt = low temperature) was revealed and this “breathing” phenomenon remains a rarity even after two decades. A superhydrated “open” phase was obtained by immersing MIL-53(Cr) in water and was reported in 2011.¹⁶⁷

Gas sorption studies involving N_2 , H_2 , CH_4 and CO_2 on MIL-53(Cr, Al) revealed guest-dependent sorption profiles.^{69,156,157} For N_2 , H_2 and CH_4 , the sorption isotherms are type I as expected for rigid microporous CNs and zeolites (Fig. 2a). In contrast, for CO_2 MIL-53(Cr, Al) were observed to exhibit type F-I sorption isotherms (Fig. 6a).⁶⁹ This was attributed to CO_2 molecules interacting strongly with the hydroxide moieties that line the rhombic tunnels, resulting in pore contraction at low pressure and pore opening at high pressure.¹⁶⁸ A two-step type F-I isotherm was observed with polar vapours (*e.g.* MeOH, EtOH) and $\text{C}_2\text{–C}_8$ hydrocarbon sorbates.^{169–171}

Substitution of the metal nodes by Fe(III) or Sc(III) resulted in nonporous “closed” phases in MIL-53(Fe or Sc) after activation.^{122,123,172} Compared to MIL-53(Sc), MIL-53(Fe) has been more widely subjected to study. CO_2 sorption on MIL-53(Fe) revealed a multi-step type F-IV^m isotherm (Fig. 6b).¹⁰⁷ Other gases such as light hydrocarbons were observed to exhibit the same trend but with

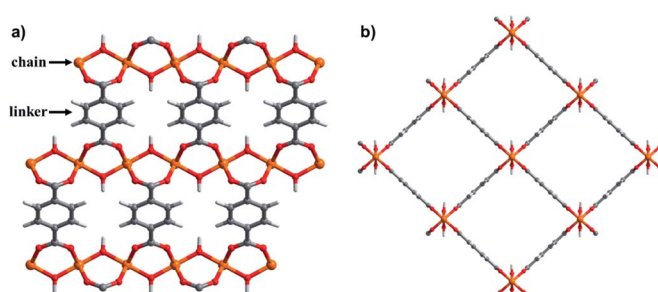


Fig. 5 Crystal structures of MIL-53(M): (a) $[\text{MO}_4(\text{OH})_2]$ chains connected by bdc linkers; (b) 1D rhombic channels in the open phase, guest molecules are omitted for clarity. Orange: M (Cr, Al, Fe, etc.), red: O, grey: C, light grey: H.



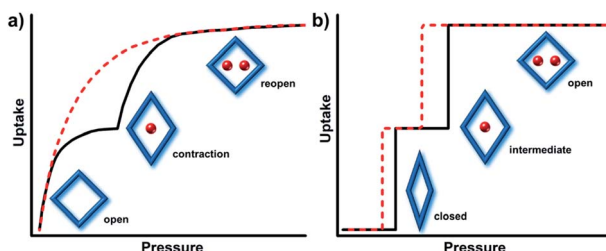


Fig. 6 Schematic illustrations of the sorption isotherm types reported for the MIL-53(M) family. (a) Type F-I isotherms with open to less open to open transformations as observed in MIL-53(Cr, Al); (b) type F-IV^m isotherm with closed to open to more open transformations as seen for MIL-53(Fe, Sc). Black solid line: adsorption curve; red dash line: desorption curve.

adsorbate-dependent switching pressures and uptakes (Fig. 7a).¹⁰⁶ The structural transformations of MIL-53(Fe) involve at least two intermediate phases (ip1 and ip2) in between its closed (cp) and open (op) phases (Fig. 7b). A variety of liquid organics, including protic/nonprotic and polar/nonpolar molecules, resulted in various degrees of expansion in MIL-53(Fe).¹⁷³ Increases in volume per formula unit ($V_{f.u.}$) between the closed and various open phases varied from 2 to 77% (Table 2).

Ligand functionalization impacts the flexibility of MIL-53(Fe) with various adsorbates (Table 3) as exemplified by MIL-53(Fe)-X variants prepared from a library of functionalised bdc ligands (Fig. 8a).^{179–183} Except for MIL-53(Fe)-2OH, the activated “dry” phases of MIL-53(Fe)-X exhibited larger volumes than MIL-53(Fe), consistent with the ip1 or ip2 phase of MIL-53(Fe) (Fig. 8b, black line).¹⁸¹ 77 K N_2 sorption studies revealed no porosity (closed phases) except for MIL-53(Fe)-2CF₃. The larger pore volumes of activated MIL-53(Fe)-X phases were attributed to steric hindrance between functional groups which prevent pore closure. Hydration was found to result in only negligible changes to the unit-cell volumes (Fig. 8b, red line). MIL-53(Fe)-2OH is an exception as it was found to exhibit high water uptake thanks to hydrogen bonding between hydroquinolic OH groups and water molecules. Regarding other solvents, MIL-53(Fe)-2COOH was observed to be an outlier. It remained in its closed phase regardless of the liquid used and exhibited no significant solvent uptake. This outcome was

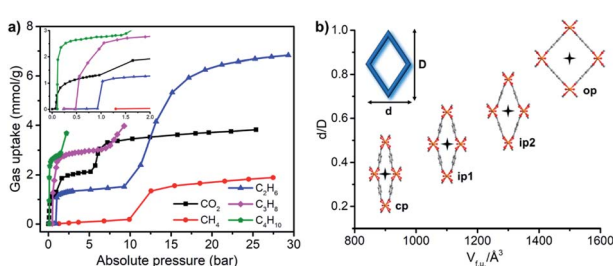


Fig. 7 (a) Gas sorption isotherms recorded for MIL-53(Fe) at 303 K; (b) different phases observed in MIL-53(Fe), cp = closed phase, ip = intermediate phase, op = open phase.



Table 2 Guest sorption studies on MIL-53(Fe) and the corresponding volumes per formula unit of guest-loaded phases^a

Guests	$V_{f.u.} (\text{\AA}^3)$	Year	Ref.
py	1393	2005	158
Closed phase/H ₂ O	900/987	2008	172
IPA/DMSO/py/DMF/quinone/THF	1271/1304/1395/1398/1455/1471	2008	173
CHCl ₃ /DEF/EA/NB/toluene/EtOH	1534/1534/1566/1581/1582/1585		
DMC/MeOH/BuOH/lutidine/MeCN/MX	1588/1591/1592/1593/1594/1587		
Ibuprofen	1407	2008	174
CH ₄	964	2009	106
C ₂ H ₆ (three phases)	984/1186/1587		
C ₃ H ₈ (three phases)	1001/1272/1565		
C ₄ H ₁₀ (three phases)	1014/1311/1566		
Lutidine/py/H ₂ O	1213/1398/1000	2010	175
MeOH (two phases)	1192/1595	2011	176
EtOH (two phases)	1199/1580		
1-PrOH (two phases)	1243/1511		
2-PrOH	1271		
OX/MX/PX	1579/1584/1582	2012	177
bzta/bztp	1590/1591	2013	178
CO ₂ (three phases)	917/1083/1563	2015	107

^a py = pyridine; IPA = isopropanol; DMSO = dimethyl sulfoxide; DMF = *N,N'*-dimethylformamide; THF = tetrahydrofuran; DEF = *N,N'*-diethylformamide; EA = ethyl acetate; NB = nitrobenzene; DMC = dimethyl carbonate; MX = *meta*-xylene; OX = *ortho*-xylene; PX = *para*-xylene; bzta = benzothiazole; bztp = benzothiophene.

attributed to strong intraframework hydrogen bonding interactions that drive the pores to remain closed. In general, pore opening in functionalised MIL-53(Fe)-X variants is governed by a balance between the intrinsic stability of the closed and open phases and guest-framework interactions. The influence of the linker on the switching of MIL-53(Fe) upon CO₂ and C₁–C₉ hydrocarbon adsorption was also systematically studied (Fig. 8c).^{182,183} With the exception of methane, closed to open transformations occurred through an intermediate phase (X= Cl, Br, CH₃), thus differing from the parent, MIL-53(Fe), for which two intermediate phases were observed (Fig. 8b). MIL-53(Fe)-2COOH and MIL-53(Fe)-NH₂ remained closed when exposed to CO₂ or hydrocarbons.^{182,183} A combination of steric effects and intraframework interactions in MIL-53(Fe)-X was deemed responsible for these observations.

Table 3 Chronology of MIL-53(Fe)-X variants

MIL-53(Fe)-X	Guests	Year	Ref.
2COOH	H ₂ O	2004	179
NH ₂	H ₂ BDC-NH ₂	2008	180
Cl, Br, NH ₂ , CH ₃ , 2OH, 2CF ₃ ,	H ₂ O, pyridine, EtOH, tetrachloroethane	2010	181
2COOH			
Cl, Br, NH ₂ , CH ₃	CH ₄ , C ₂ H ₆ , C ₃ H ₈ , C ₄ H ₁₀ , C ₆ H ₁₄ , C ₇ H ₁₆ , C ₈ H ₁₈ , C ₉ H ₂₀	2011	182
Cl, Br, NH ₂ , CH ₃ , 2COOH	CO ₂	2012	183



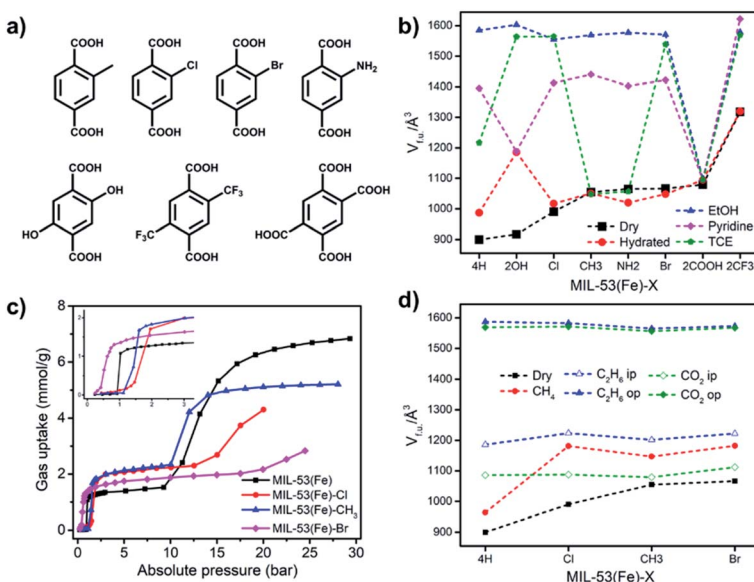


Fig. 8 (a) The functionalised bdc ligands used to synthesise MIL-53(Fe)-X variants; (b) and (d) volume per formula unit ($V_{f.u.}$) of MIL-53(Fe)-X variants under different conditions, 4H = MIL-53(Fe); (c) C_2H_6 sorption isotherms of MIL-53(Fe)-X at 303 K.

2.1.2 Pillared-layer CNs. Pillared-layer coordination networks (PLCNs) are a diverse class of CNs that have been extensively studied in the past two decades.^{6,184–188} Most PLCNs feature **pcu** or “jungle-gym” geometry and the most commonly studied subset has the general formula $[M_2L_2P]_n$ (M = divalent metal cation; class I: L = dicarboxylate linker and P = N-donor pillar; class II: L = N-donor linker and P = inorganic anionic pillar).¹⁸⁸ Class I PLCNs comprise two-dimensional **sql** topology networks linked by dicarboxylate linker ligands (L) which are pillared in the third dimension by neutral N-donor linker ligands (P) to form **pcu** topology frameworks (Fig. 9). The metal nodes of the prototypal PLCNs are dinuclear paddle-wheel $[M_2(COO)_4]$ that serve as 6-connected (6c) MBBs.

The prototypal PLCN, $[Zn_2(bdc)_2(dabco)]_n$ (dabco = 1,4-diazabicyclo[2.2.2]octane), is widely known as DMOF-1. The bdc-linked **sql** nets are comprised of

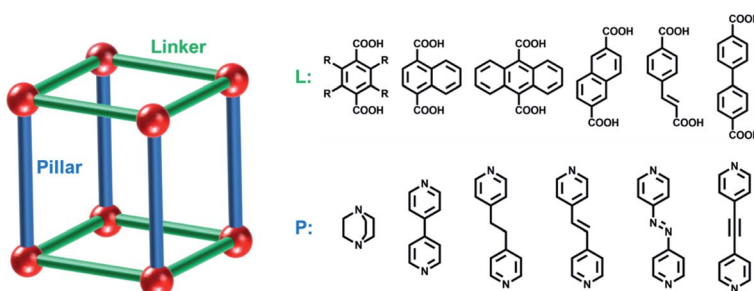


Fig. 9 Schematic illustration of pillared-layer coordination networks with examples of linker (L) and pillar ligands (P).



[Zn₂(COO)₄] paddle-wheel moieties that are pillared by dabco ligands to form the resulting **pcu** framework.^{189–192} Sorption studies using N₂ and H₂ on DMOF-1 revealed type I isotherms, an indication of structural rigidity.¹⁸⁹ However, benzene was found to induce structural deformation of DMOF-1 from square to rhombic grids. Interestingly, sorption of IPA, MeOH and EtOH on DMOF-1 afforded two-step type F-I isotherms.^{190,191} The first step resulted from contraction whereas the second step corresponded to pore reopening. Molecular simulations have provided insight into these structural changes.¹⁹²

The ready availability/accessibility of numerous dicarboxylic acids and dipyrromethane ligands has enabled facile linker and pillar functionalization/substitution of DMOF-1 to create families of related **pcu** structures. In addition, Zn(II) can be replaced by several other transition metals. Studies on the sorption properties of DMOF-1 derivatives have revealed profound effects upon sorption profiles.^{51,71,93,97–99,113–121,146,147} For example, the DMOF-1 analogue [Ni₂(ndc)₂(dabco)]_n (ndc = 1,4-naphthalenedicarboxylate), DUT-8(Ni), was reported to exhibit large and reversible expansion/shrinkage between its closed and open phases.^{113–117} Introduced by Kaskel's group in 2010, DUT-8(Ni) is isostructural to DMOF-1, the main difference being the length of linker ligands. The longer ndc linker in DUT-8(Ni) not only leads to larger pores and higher sorption uptakes, but results in single-step type F-IV^s isotherms induced by N₂, Xe, CO₂ and *n*-butane.¹¹³ As-synthesised DUT-8(Ni) transforms to its closed phase during desolvation accompanied by a colour change from green to yellow. Compared to its open phase, the paddle-wheel units in the closed phase are strongly distorted (Fig. 10a and b) and the N–Ni–Ni–N atoms of paddle-wheel units and dabco molecules are arranged in zigzag rather than linear fashion (Fig. 10c and d).¹¹⁵ Induced by guest sorption, the structural transformation from closed ($V_{f.u.} = 648 \text{ \AA}^3$) to open ($V_{f.u.} = 1644 \text{ \AA}^3$) phases involves >150% volume expansion without covalent bond breakage (Fig. 10e and f), one of the largest volume changes reported for flexible CNs. This large expansion enables exceptionally high N₂ ($\sim 700 \text{ cm}^3 \text{ g}^{-1}$) and CO₂ ($\sim 600 \text{ cm}^3 \text{ g}^{-1}$) uptakes (Fig. 10g).

Kaskel's group subsequently reported that other metals can sustain DUT-8(M) analogues (M = Co, Zn, Cu) and exhibit distinct sorption profiles.¹¹⁴ Depending on the metal ion used, DUT-8 variants were found to exhibit reversible (DUT-8(Ni), DUT-8(Co)), irreversible (DUT-8(Zn)) or no (DUT-8(Cu)) transformation upon

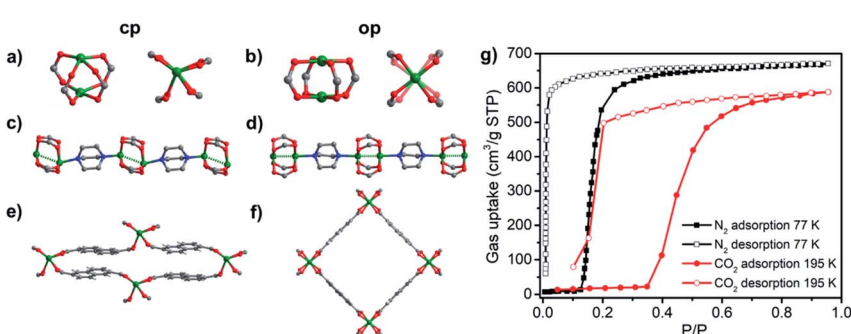


Fig. 10 Comparison of the closed (a, c, e) and open (b, d, f) phases of DUT-8(Ni); (g) N₂ (77 K) and CO₂ (195 K) sorption isotherms of DUT-8(Ni).



activation and/or guest sorption. It was noted that the particle size of DUT-8(Ni) can influence sorption profiles, which were either type F-IV^s (particle size $> 1 \mu\text{m}$) or type I (particle size $< 500 \text{ nm}$).^{116,193,194} A similar “downsizing” effect was also reported for the DMOF-1 analogue $[\text{Cu}_2(\text{bdc})_2(\text{bpy})]$.⁹³

Recently, our group reported the structures and sorption properties of a series of DMOF-1 variants, namely $[\text{Zn}_2(\text{DMTDC})_2(\text{P})]$, X-pcu-*n*-Zn (*n* = 5, P = 1,2-di(4-pyridyl)-ethylene (dpe); *n* = 6, P = 1,2-bis(4-pyridyl)ethane (bpe); *n* = 7, P = 1,2-bis(4-pyridyl)acetylene (bpa); *n* = 8, P = 4,4'-azopyridine (apy); H₂DMTDC = 3,4-dimethylthieno[2,3-*b*]thiophene-2,5-dicarboxylic acid).^{146,147} The four pillar ligands used are longer than dabco and enable 2-fold interpenetration in the X-pcu-*n*-Zn family (Fig. 11a). The as-synthesised “open” phases, X-pcu-*n*-Zn- α , were obtained by solvothermal synthesis with solvent molecules occupying voids and calculated guest-accessible volumes of *ca.* 45% (Fig. 11b). Single-crystal X-ray diffraction (SCXRD) studies revealed that activation of X-pcu-*n*-Zn- α resulted in “closed” nonporous phases, X-pcu-*n*-Zn- β , with unit cell volumes reduced by *ca.* 35% (Fig. 11c). CO₂, C₂H₂ and C₂H₄ sorption on X-pcu-*n*-Zn- β revealed switching behaviour with comparable uptakes but different switching pressures (Fig. 11d–f). Up to 250 cm³ g⁻¹ CO₂ uptake and good recyclability (>35 sorption cycles) make X-pcu-*n*-Zn only the second family of flexible CNs to exhibit both high uptake and reversibility. The switching pressures for the three gases studied followed a consistent trend: X-pcu-6-Zn- β < X-pcu-5-Zn- β < X-pcu-7-Zn- β < X-pcu-8-Zn- β which was attributed to the relative degree of conformational flexibility of the pillar ligands.¹⁴⁷

By exploring longer linkers and extended pillar ligands, other interpenetrated derivatives of DMOF-1 have been obtained. For example, with 4,4'-biphenyldicarboxylate as the linker and 1,4-bis(4-pyridyl)benzene or 4,4'-bis(4-pyridyl)biphenyl as the pillar, 3-fold interpenetrated CNs X-pcu-3-Zn and X-pcu-1-Zn were synthesised, respectively.^{73,195} Although interpenetration inevitably reduces guest-accessible voids, X-pcu-3-Zn and X-pcu-1-Zn nevertheless exhibited *ca.* 45%

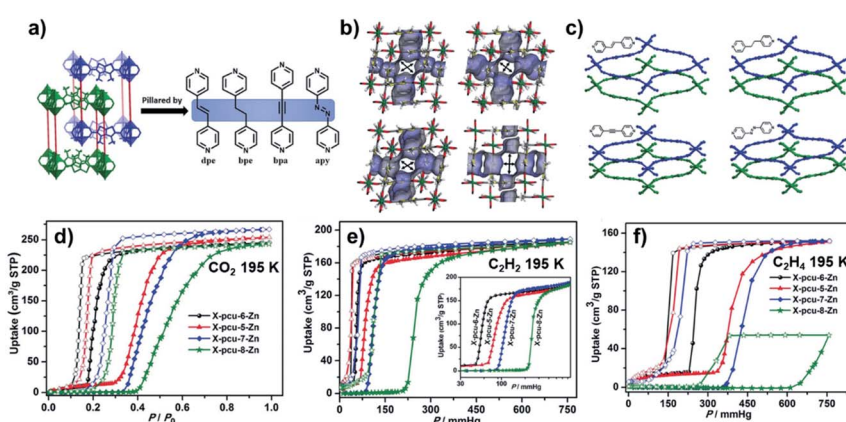


Fig. 11 (a) The two-fold interpenetrated structures of X-pcu-*n*-Zn; (b) as-synthesised “open” phases, X-pcu-*n*-Zn- α ; (c) activated “closed” phases, X-pcu-*n*-Zn- β ; (d–f) CO₂, C₂H₂ and C₂H₄ sorption isotherms on X-pcu-*n*-Zn- β at 195 K. Reproduced from ref. 147 with permission; copyright: 2019, John Wiley & Sons, Inc.



guest-accessible volume. Both PLCNs were found to exhibit complicated structural transformations through solvent exchange, heating, vacuum and gas sorption processes. Interestingly, a rare example of “shape memory” was observed for X-pcu-3-Zn and X-pcu-1-Zn, which exhibited irreversible phase transitions. The only other reported example of this phenomenon was for $[\text{Cu}_2(\text{bdc})_2(\text{bpy})]^{93}$.

A second diverse class of PLCNs is exemplified by the SIFSIX-*n*-M family of general formula $[\text{M}(\text{L})_2(\text{SiF}_6)]$ (M = divalent transition metal ions, L = N-donor ditopic ligands).⁶ This family is diverse in composition since the SIFSIX pillar can be replaced by other fluorinated divalent anions such as TiF_6^{2-} , GeF_6^{2-} and SnF_6^{2-} and there are numerous N-donor linkers available. A difference between the SIFSIX-*n*-M and DMOF-1 families is that N-donor ligands act as linkers in the former whereas they serve as pillars in the latter. Cationic **sql** layers in the SIFSIX-*n*-M family are charge balanced by anionic pillars. The SIFSIX-*n*-M family is of particular interest because several members have been reported to exhibit benchmark separation performances towards a variety of gas mixtures.^{196,197} Whereas SIFSIX-*n*-M sorbents generally remain rigid during sorption cycles, rotation of linkers can cause inflections in gas adsorption isotherms.^{198,199} Recently, our group introduced the first switching SIFSIX-*n*-M PLCN, $[\text{Cu}(\text{L})_2(\text{SiF}_6)]$ (SIFSIX-23-Cu, L = 1,4-bis(1-imidazolyl)benzene), which was found to exhibit dramatic structural distortions.¹⁵¹ Unlike previous SIFSIX-*n*-M sorbents, the SIFSIX pillars in SIFSIX-23-Cu adopt a *cis*-bridging mode (Fig. 12a and b) and the **sql** layers undulate thanks to the “V”-shaped *L*(*syn*) linker ligands (Fig. 12c). Desolvation induces SIFSIX-23-Cu to undergo structural transformations involving multiple intermediate phases (SIFSIX-23-Cu- γ 1, - γ 2, - γ 3) prior to forming a solvent-free closed phase, SIFSIX-23-Cu- β 1 (Fig. 12d). N_2 and CO_2 sorption on SIFSIX-23-Cu- β 1 reveal type F-IV^s and type F-IV^m isotherms,

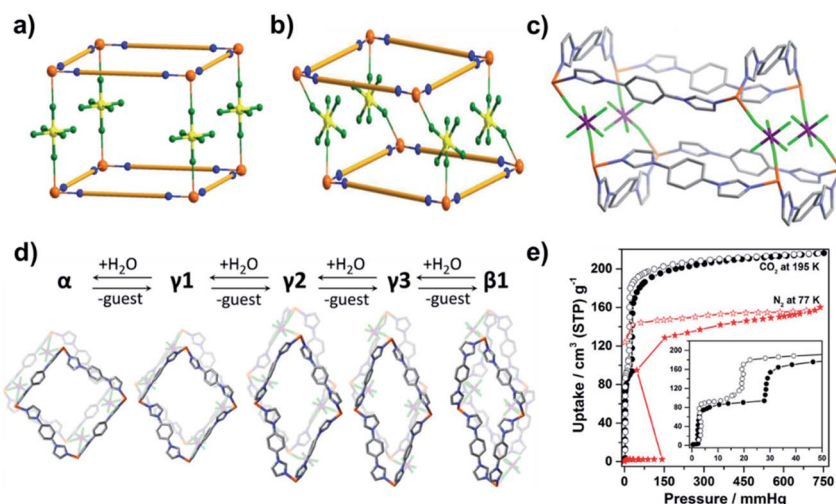


Fig. 12 Schematic diagrams of (a) traditional SIFSIX-*n*-M networks with *trans*-bridging SIFSIX pillars and (b) SIFSIX-23-Cu with *cis*-bridging SIFSIX pillars; (c) coordination mode and geometry in SIFSIX-23-Cu; (d) reversible structural transformations in SIFSIX-23-Cu; (e) N_2 (77 K) and CO_2 (195 K) sorption isotherms of SIFSIX-23-Cu. Reproduced from ref. 151 with permission; copyright: 2020, American Chemical Society.



respectively (Fig. 12e). SIFSIX-23-Cu is one of the few switching CNs that exhibits $>200 \text{ cm}^3 \text{ g}^{-1}$ gas uptake and good recyclability (>40 sorption cycles). SIFSIX-23-Cu was also found to be stable in water for at least one year.

2.1.3 Diamondoid CNs. Diamondoid CNs feature **dia** topology and are amongst the earliest and most comprehensively studied CNs. They are also highly amenable to crystal engineering.^{13,14,200,201} Interpenetration in diamondoid CNs tends to reduce surface area but can enhance rigidity.²⁰² Nevertheless, structural flexibility was observed in the 2-fold interpenetrated diamondoid CN [In(ABDC)₂] (SHF-61, ABDC = 2-aminobenzene-1,4-dicarboxylate) with continuous breathing/swelling behaviour during desolvation/solvation.²⁰³ This is a rare phenomenon that was previously observed in MIL-88 CNs.^{56,57} The 8-fold interpenetrated diamondoid CN [Zn(oba)(pip)] (JUK-8), which is based on 4,4'-oxybis(benzenedicarboxylate) (oba) and 4-pyridyl functionalised benzene-1,3-dicarbohydrazide (pip) linkers, exhibited switching upon exposure to H₂O and CO₂.¹⁵⁴

Recently, our group reported a flexible diamondoid CN [NiL₂], X-dia-1-Ni, which is based upon a mixed N/O-donor ligand, 4-(4-pyridyl)-biphenyl-4-carboxylic acid (HL).⁶⁷ Despite 6-fold interpenetration, the accessible void volume in X-dia-1-Ni is 49% thanks to the mode of interpenetration and the rectangular channels sustained by ligand L (Fig. 13a-d). X-dia-1-Ni was observed to undergo single-crystal-to-single-crystal (SCSC) transformations through solvent exchange with CH₂Cl₂ and transform to its closed phase X-dia-1-Ni-c1 by heating under vacuum (Fig. 13e). 77 K N₂ sorption indicated that X-dia-1-Ni-c1 is nonporous whereas 195 K CO₂ sorption revealed multiple steps in both the adsorption and desorption branches. These profiles indicate reversible structural

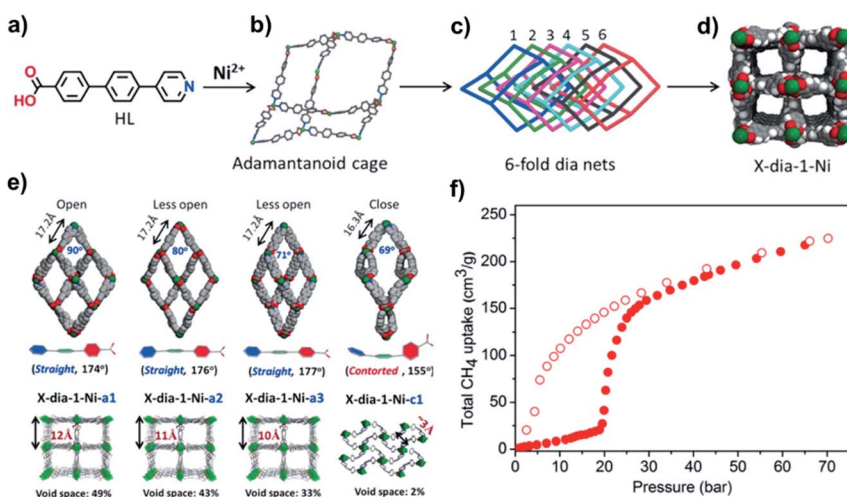


Fig. 13 (a) Structure of 4-(4-pyridyl)-biphenyl-4-carboxylic acid (HL); (b) adamantanoid cage in X-dia-1-Ni; (c) 6-fold interpenetrated dia nets in X-dia-1-Ni; (d) rectangular channels of X-dia-1-Ni viewed along the c-axis; (e) single crystal structures of the porous (a1, a2, a3) and nonporous (c1) phases of X-dia-1-Ni; (f) high pressure CH₄ sorption isotherm of X-dia-1-Ni at 298 K. Reproduced from ref. 67 with permission; copyright: 2018, John Wiley & Sons, Inc.



changes between closed and open phases. Interestingly, the CH_4 adsorption isotherm measured at 298 K (Fig. 13f) revealed a type F-IV^s isotherm that combined an appropriate switching pressure (5–35 bar) and high saturation uptake ($>200 \text{ cm}^3 \text{ g}^{-1}$). These metrics made X-dia-1-Ni only the second flexible CN after Co(bdp) to exhibit such a high working capacity for CH_4 . Co(bdp) is discussed in the following section.

2.1.4 M(bdp) family. Switching CNs usually exhibit only two phases (*e.g.* one open phase and one closed phase) and their structural transformations are typically induced by polar gases such as CO_2 and C_2H_2 or polar solvents. Multiple phase transitions induced by nonpolar molecules such as H_2 and N_2 are somewhat rare. Long *et al.* reported that a 3D switching CN Co(bdp) (Fig. 14a, bdp = 1,4-benzenedipyrrolotriphosphazolate),^{74,101–103} exhibits an unusual five-step N_2 sorption isotherm at 77 K (Fig. 14b). A combination of *in situ* PXRD and molecular simulation studies revealed that the activated “closed” phase, Co(bdp)-dry, transformed to its fully “open” phase *via* three distinct intermediate phases (Fig. 14c). In addition, H_2 sorption on Co(bdp)-dry revealed a phase transformation which was not seen in other switching CNs.¹⁰¹ Most importantly, Co(bdp)-dry exhibits a stepped type F-IV^s isotherm when exposed to CH_4 (Fig. 14d).⁷⁴ The gate adsorption and desorption pressures are *ca.* 15 and 5 bar, respectively, suitable for CH_4 storage and delivery in the context of vehicular transport (5–35 bar). High uptake and the right type of F-IV isotherm profile made Co(bdp) the benchmark for CH_4 working capacity (*ca.* $200 \text{ cm}^3 \text{ cm}^{-3}$). The Fe

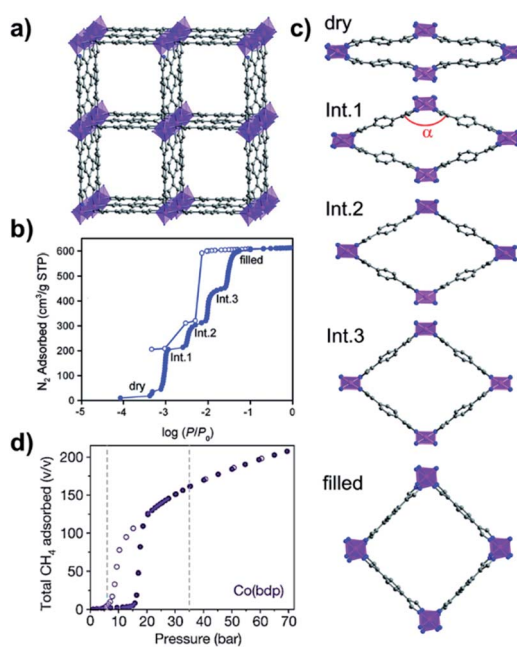


Fig. 14 (a) Crystal structure of as-synthesised Co(bdp); (b) N_2 sorption isotherms of Co(bdp)-dry at 77 K; (c) phase transition during N_2 sorption; and (d) CH_4 sorption isotherms of Co(bdp)-dry at 298 K. Reproduced from ref. 74 and 102 with permission; copyrights: 2015, Springer Nature and 2010, American Chemical Society.



analogue, Fe(bdp), was also found to exhibit a type F-IV^s isotherm but with a much higher switching pressure, highlighting the profound impact that metal centers can exert on switching pressures. In contrast, the Zn and Ni analogues, Zn(bdp) and Ni(bdp), were only found to exhibit type I gas sorption isotherms.²⁰⁴ Furthermore, ligand functionalization in Co(bdp) can be used to tune the switching pressures.¹³³

2.2. Examples of 2D switching CNs

2.2.1 Square lattice (sql) CNs. 2D CNs may exhibit switching through clay-like intercalation. One would intuitively anticipate that such a switching mechanism is facile because the attractive forces between layers are relatively weak and little strain upon the CN is likely to be required. Square lattice (**sql**) CNs are quite prevalent and account for nearly half of reported 2D CNs.²⁰⁵ A well-studied family of **sql** CNs is comprised of octahedral metal ions (M), axial counter anions (A) and linear linker ligands (L).²⁰⁶ When M : L is 1 : 2, **sql** CNs of general formula $[M(L)_2(A)_2] \cdot x\text{guest}$ can be formed (Fig. 15).^{207–209} From a crystal engineering perspective, this family of CNs exemplify the “node and linker” strategy first developed by Robson and Hoskins over thirty years ago.^{13,14} An emphasis upon design and structural characterization of **sql** CNs preceded sorption studies until the ELM (elastic layer-structured MOF) family was investigated.^{28,59,72,85–90}

The first reported sorption study on **sql** CNs was conducted upon $[\text{Cu}(\text{bpy})_2(\text{BF}_4)_2]$, ELM-11.⁵⁹ In 2001, Kaneko *et al.* first studied the 1D linear chain CP $[\text{Cu}(\text{bpy})(\text{BF}_4)_2(\text{H}_2\text{O})_2 \cdot \text{bpy}]$ (Fig. 16a)²⁸ and its activated form, ELM-11, was observed to exhibit phase switching when exposed to N₂, Ar and CO₂. To our knowledge, this is the first example of type F-IV sorption isotherms in switching CNs. This behaviour was initially attributed to hydrogen bond regulation but there was no structural information concerning the activated form.²⁸ It was not until 2006 that the structure of the activated form was determined by synchrotron PXRD to be the **sql** topology CN $[\text{Cu}(\text{bpy})_2(\text{BF}_4)_2]$ (Fig. 16b).⁸⁸ It was later found that ELM-11 underwent a multi-step rather than single-step phase transition induced by CO₂ at 1 bar when the temperature was decreased from 273 to 195 K (Fig. 16c),^{86,87} revealing a type F-IV^m isotherm. The mechanism of the switching behaviour was reinterpreted as expansion/shrinkage between adjacent layers triggered by inclusion of CO₂ molecules (Fig. 16d).

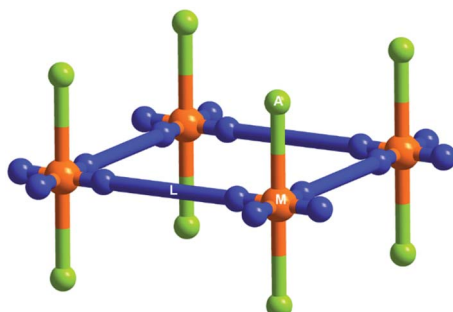


Fig. 15 A schematic illustration of 2D **sql** CNs. Orange balls: octahedral metal ions (M), lime balls: axial counter anions (A), blue rods: linear linker ligands (L).



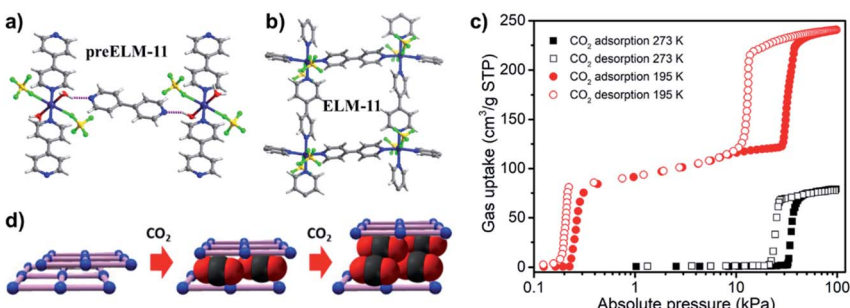


Fig. 16 The structures of (a) preELM-11 and (b) ELM-11; (c) CO_2 sorption isotherms of ELM-11 at 195 and 273 K; and (d) illustration of expansion/shrinkage of the adjacent layers in ELM-11. Figure (d) is reproduced from ref. 86 with permission; copyright: 2016, American Chemical Society.

Substitution of the metal cations or counter anions afforded several ELM-11 analogues,^{59,89} including $[\text{Cu}(\text{bpy})_2(\text{OTf})_2]$ (ELM-12),⁷⁰ $[\text{Cu}(\text{bpy})_2(\text{BF}_3\text{CF}_3)_2]$ (ELM-13),¹⁵³ and $[\text{Ni}(\text{bpy})_2(\text{BF}_4)_2]$ (ELM-31).¹⁰⁴ ELM-12 exhibited an open phase after guest removal, possibly because of the “pillaring” role of the OTf^- anions. With respect to N_2 sorption, ELM-12 exhibited a two-step type F-II isotherm distinct from that observed in ELM-11. On the other hand, both ELM-13 and ELM-31 were observed to exhibit type F-IV isotherms like ELM-11 but with different uptakes and switching pressures.

Recently, our group studied the sorption properties of the previously known **sql** CN $[\text{Co}(\text{bpy})_2(\text{NCS})_2]$,²⁰⁸ **sql-1-Co-NCS**,^{144,145} which is isostructural to the ELM family. **sql-1-Co-NCS** is sustained by $\text{Co}^{(II)}$ ions coordinated at equatorial coordination sites to bpy linker ligands with terminal NCS^- anions occupying the axial positions. Whereas the N_2 uptake of **sql-1-Co-NCS** at 77 K was found to be negligible (Fig. 17a), the 195 K CO_2 isotherm was observed to exhibit a type F-IV⁸ isotherm.¹⁴⁴ Such an isotherm is consistent with the switching behaviour seen in ELM-11. High-pressure CO_2 sorption isotherms of **sql-1-Co-NCS** were recorded at different temperatures and the relationship between temperature and switching pressure was found to obey the Clausius–Clapeyron equation. In addition, recyclability tests revealed that **sql-1-Co-NCS** exhibits good recyclability and fast kinetics. C_8 aromatic vapour sorption isotherms were also collected on **sql-1-Co-NCS** at 298 K (Fig. 17b).¹⁴⁵ It was observed that **sql-1-Co-NCS** switches in the presence of each of the C_8 aromatic isomers but with marked differences in terms of adsorption capacity and switching pressure. Single-crystal and powder XRD studies revealed that the interlayer distance in the closed phase (4.5 Å) increased to 5.4 Å (CO_2 loaded phase) and to 9.2 Å (xylene loaded phase) (Fig. 17c–e), the largest interlayer separation yet reported for bpy-based **sql** CNs.

2.2.2 Other examples of switching 2D CNs. Kitagawa and co-workers documented several examples of 2D interdigitated layered CNs and studied their switching properties.^{65,66} $[\text{Cu}(\text{dhbc})_2(\text{bpy})]$ was prepared from copper nitrate, 2,5-dihydroxybenzoic acid (Hdhbc) and 4,4'-bipyridine (bpy). $\text{Cu}^{(II)}$ ions are linked by bpy linkers to generate chains that are further linked by two carboxyl groups of dhbc to afford a 2D layer motif.⁶⁵ These layers are mutually interdigitated by the



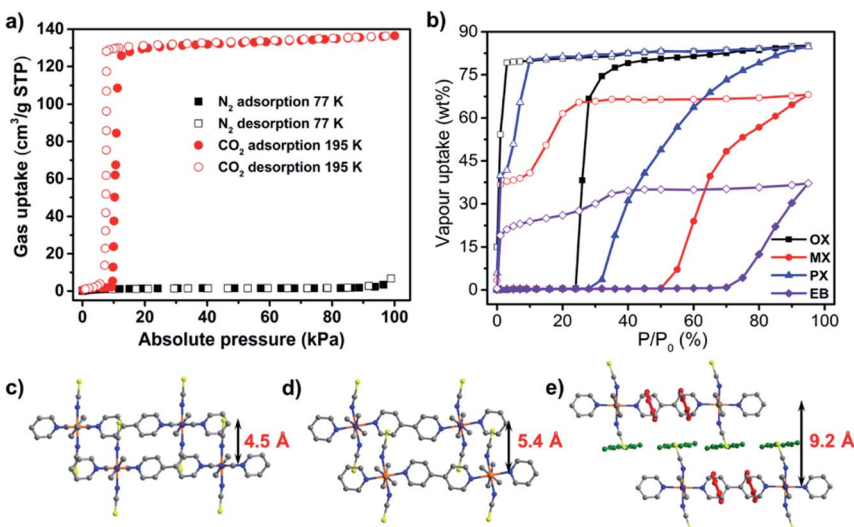


Fig. 17 (a and b) N₂ (77 K), CO₂ (195 K) and C₈ vapour (298 K) sorption isotherms for sql-1-Co-NCS; (c–e) layer packing of nonporous, CO₂-loaded and xylene loaded phases of sql-1-Co-NCS, respectively.

phenolic group of dhbc to generate 1D channels (Fig. 18a). Despite no change to the Cu(II) coordination environment after activation, the dhbc ligands tilt significantly and transform from *cis*-mode to *trans*-mode arrangement which results in layer shrinkage (Fig. 18b).⁹⁴ High pressure N₂, O₂, CH₄ and CO₂ sorption studies demonstrated that the activated phase of [Cu(dhbc)₂(bpy)] exhibits a switching effect with type F-IV⁸ isotherms (Fig. 18c). This study was the first report of a stepped sorption in switching CNs at ambient temperature and high pressure. Adsorbate-dependent switching pressures were observed at 50, 35 and 0.4 bar for N₂, O₂ and CO₂, respectively.

In 2008, Kitagawa's group introduced another 2D interdigitated CN, [Cd(bpndc)(bpy)] (bpndc = benzophenone-4,4'-dicarboxylate).⁶⁶ SCXRD studies revealed that Cd(II) nodes are linked by bpndc ligands to produce 1D double-chain

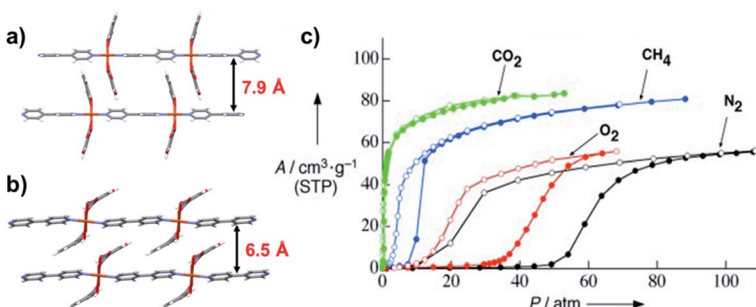


Fig. 18 Crystal structures of (a) open and (b) closed phases of [Cu(dhbc)₂(bpy)] and (c) high pressure gas sorption isotherms of its activated phase at 298 K. Figure (c) is reproduced from ref. 65 with permission; copyright: 2003, John Wiley & Sons, Inc.



structures of $[\text{Cd}(\text{bpndc})]$ (Fig. 19a), which are in turn linked by bpy to afford a 2D bilayer motif (Fig. 19b). As-synthesised $[\text{Cd}(\text{bpndc})(\text{bpy})]$ underwent a significant contraction through activation to form its closed phase (Fig. 19c). The sorption isotherms at 90 K revealed type F-IV^s isotherms with different switching pressures for O_2 , Ar and N_2 of 3.9, 40.1 and 55.3 kPa (Fig. 19d), respectively.

2.3. Factors that impact switching between phases

Various factors can influence the flexibility of switching CNs. With respect to extrinsic factors, temperature, pressure and the nature of the adsorbate all impact switching events. Since switching between the closed and open phases is generally a thermodynamic event, low temperature and high pressure tend to promote more facile switching. To this end, in order to screen for switching it is recommended that sorption isotherms are collected at the boiling point of the adsorbate (e.g. 77 K for N_2 or 195 K for CO_2). High-pressure gas sorption might be necessary at ambient temperatures. For example, at 298 K and 1 bar, sql-1-Co-NCS does not exhibit switching upon exposure to CO_2 . Rather, switching requires either decreasing the temperature to 195 K or increasing pressure to around 30 bar.¹⁴⁴ The adsorbate is also a key factor since adsorbate–adsorbent interactions play a role in triggering the phase transformations.¹⁰⁶ In general, nonpolar gases such as H_2 , Ar , O_2 and N_2 tend to exhibit relatively weak interactions with most CNs. Hydrocarbons with unsaturated bonds may favour host–guest interactions with decreasing affinity as follows: aromatics > alkynes > alkenes > alkanes. The number of carbon atoms of hydrocarbon adsorbates also influences switching since more carbon atoms generally results in stronger host–guest interactions. However, this empirical rule-of-thumb is limited by the need for suitable pore size and shape in the open phase of switching CNs.

With respect to intrinsic factors, the composition of a CN is key to enabling and controlling phase transformations including switching. Ligand functionalization has been established as an effective route to fine-tune switching pressure as demonstrated with $\text{Co}(\text{bdp})\text{-X}$ ¹³³ and $\text{MIL-53}(\text{Fe})\text{-X}$.^{182,183} Pillar ligand substitution of $\text{X-pcu-}n\text{-Zn}$ PLCNs was also effective.^{146,147} However, linker ligand

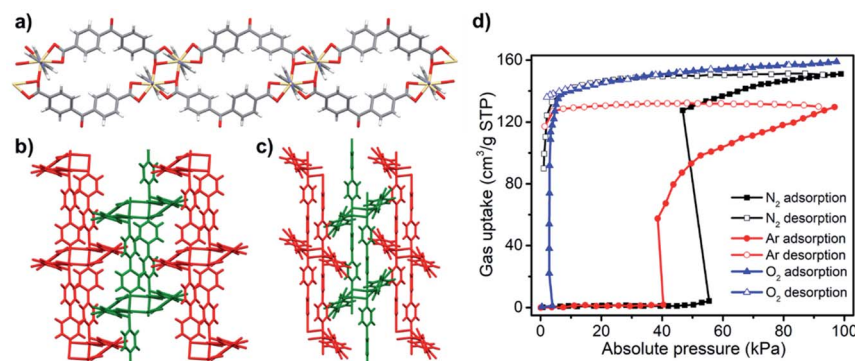


Fig. 19 (a) 1D double chain structure of $[\text{Cd}(\text{bpndc})]$; (b and c) 2D bilayer structure of as-synthesised and activated forms of $[\text{Cd}(\text{bpndc})(\text{bpy})]$; (d) O_2 , N_2 and Ar sorption isotherms recorded on activated $[\text{Cd}(\text{bpndc})(\text{bpy})]$ at 90 K.



substitution in PLCNs (*e.g.* DUT-8(Ni)^{113,114} *vs.* DMOF-1 (ref. 189–191)) can stop switching. This can also occur with metal-node substitution. For three well-studied families of switching CNs, MIL-53(M), DUT-8(M) and M(dpd), switching was profoundly affected by metal node substitution. Only specific metal nodes, *i.e.*, MIL-53(Fe/Sc), DUT-8(Ni) and Co/Fe(dpd), were observed to exhibit switching behaviour. Particle size can also impact switching behaviour but remains largely understudied.^{140,194}

3. Switching mechanisms

Although switching CNs generally exhibit type F-IV sorption isotherms and may share structural features, switching mechanisms can vary. Most switching CNs crystallize as solvated (open) phases and transform to their desolvated (closed) phases during solvent removal/activation. For some CNs this is the full scope of phases and switching occurs just between the as-synthesized (open) and activated (closed) phases. For other CNs, one or more metastable states (intermediate phases) that are partially open can exist in addition to the closed and fully open phases. To elucidate switching mechanisms we herein analyse the closed and open phases of switching CNs that are structurally characterized (usually by SCXRD). At the molecular level, switching mechanisms can be driven by intra-network distortions, inter-network interactions or most likely a combination thereof (Fig. 20 and Table 4).^{38–41} Intra-network distortions include ligand motions (Fig. 20a: bending, twisting and rotation), metal node coordination sphere changes (Fig. 20b: deformation and reconstitution/isomerism) and overall intra-network motions (Fig. 20c: edge bending/straightening and net shearing). Inter-network motions include subnetwork displacements such as interpenetrated net sliding (Fig. 20d) and layered net expansion (Fig. 20e).

Ligand motion is often observed, not just in flexible CNs, but also in rigid CNs.^{210–212} When ligand motion occurs in switching CNs it tends to occur over

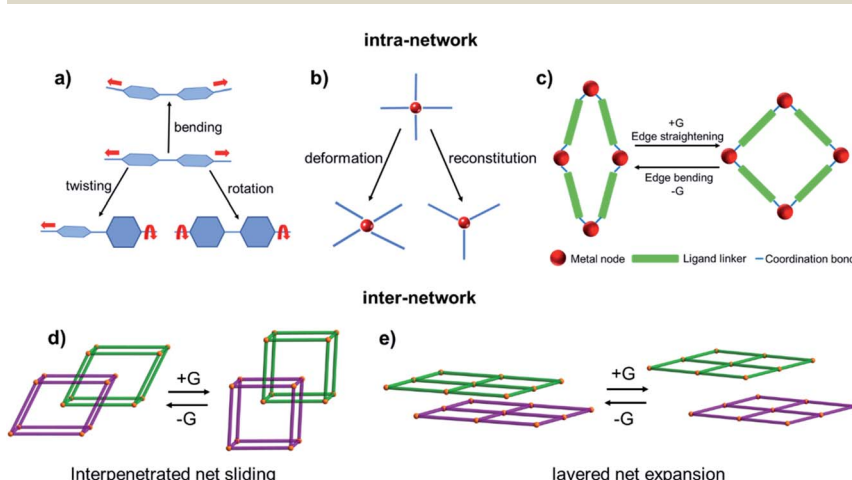


Fig. 20 Schematic of switching mechanisms driven by intra-network and inter-network changes: (a) ligand motion; (b) metal node motion; (c) overall intra-network motion; (d) interpenetrated net sliding and (e) layered net expansion.



Table 4 Switching mechanisms of representative switching CNs^a

Switching CNs	Switching mechanisms							
	Intra-network				Inter-network			
	Metal node		Linker ligand		Subnet			
	A	B	C	D	E	F	G	Ref.
MIL-53(Fe)	✗	✗	✓	✗	✗	✗	✗	106
MOF-508	✓	✗	✓	✗	✗	✓	✗	97 and 99
DUT-8(Ni)	✓	✗	✓	✗	✗	✗	✗	115
[Cu ₂ (bdc) ₂ (bpy)]	✓	✗	✓	✗	✓	✓	✗	93
[Zn ₂ (tp) ₂ (dfpbpb)]	✗	✓	✓	✓	✓	✓	✗	120
X-pcu- <i>n</i> -Zn (<i>n</i> = 5–8)	✗	✗	✓	✗	✓	✓	✗	146 and 147
X-dia-1-Ni	✗	✗	✗	✓	✓	✓	✗	67
Co(bdp)	✗	✗	✓	✗	✓	✗	✗	102
ELM-11	✗	✗	✓	✗	✓	✗	✓	89
sql-1-Co-NCS	✗	✗	✓	✗	✓	✗	✓	144 and 145
[Cu(dhbc) ₂ (bpy)]	✗	✗	✓	✗	✓	✗	✓	65 and 94
[Cu(pyrdc)(bpp)]	✗	✓	✗	✓	✗	✗	✓	96
[Cd(bpndc)(bpy)]	✗	✓	✗	✗	✗	✗	✓	66
SIFSIX-23-Cu	✗	✗	✓	✓	✓	✗	✗	151

^a A: deformation; B: reconstitution; C: rotation; D: bending; E: twisting; F: interpenetrated net sliding; G: layered net expansion.

a relatively large amplitude. Compositional analysis of switching CNs reveals that the most commonly used organic ligands are the linear linkers bpy and bdc, which occur in *ca.* 25% of switching CNs. The N-donor linker bpy can rotate and twist even without ligand bending, as exemplified by sql CNs such as sql-1-Co-NCS (Fig. 21a).^{144,145} The O-donor ligand bdc rotates, as exemplified by MIL-53(Fe) (Fig. 21b and 7b),¹⁰⁶ and bending behaviour was reported for DMOF-1.¹⁸⁹ Ligand rotation is a feature of functionalised MIL-53(Fe) analogues, MIL-53(Fe)-X, whereby the functional groups X in the closed phases project towards the channels and prevent full contraction.¹⁸¹ Ligand rotation and twisting was also reported for Co(bdp) (Fig. 21c),⁷⁴ whereas more extreme ligand bending that could be described as contortion was seen for longer ligands such as pbpc in X-dia-1-Ni (Fig. 13e).⁶⁷

Metal node motion does not always occur in switching CNs. For example, the coordination environments of metal nodes in sql-1-Co-NCS (octahedral geometry), MIL-53(Fe) (octahedral geometry) and Co(bdp) (tetrahedral geometry) were unchanged in their closed and open phases. Conversely, metal node deformation was observed in the [Zn₂(COO)₄] and [Ni₂(COO)₄] paddle-wheel units of MOF-508 (ref. 97 and 99) and DUT-8(Ni),¹¹⁵ respectively (Fig. 10a). Metal node isomerism involving coordination bond breakage remains relatively rare but plays an important role in some switching CNs, *e.g.* [Cu(pyrdc)(bpp)], [Zn₂(bdc)₂(dfpbpb)] and [Co(VTTF)].^{96,120,138}

Intra-network motion can often be attributed to cooperative ligand and metal node motions, *e.g.* net shearing and edge bending/strengthening (hinge motion)



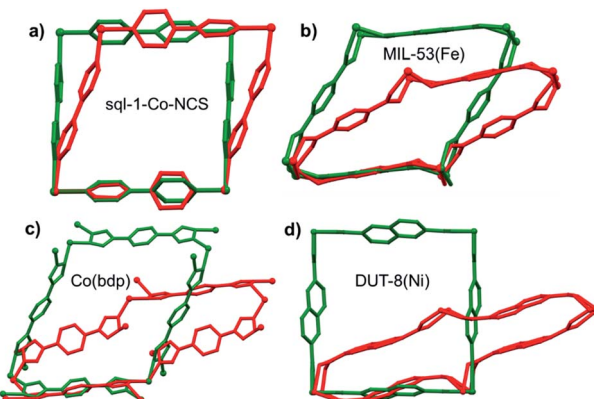


Fig. 21 Overlay comparison of closed (red) and open (green) phases of four switching CNs: (a) sql-1-Co-NCS; (b) MIL-53(Fe); (c) Co(bdp) and (d) DUT-8(Ni).

that arise thanks to nonlinear coordination modes between metal ions and organic ligands. Overall, our analysis indicates that intra-network motions are quite common in switching CNs that feature square or rhombic cavities (Fig. 21). This is presumably attributable to the rhombus being a basic flexible building block of a “truss network”, as observed even at the macro scale.²¹³ For example, at the macro scale, a common use of “rhombus deformation” in a chemistry lab would be the lab jack. Integration of square or rhombic units into a CN is likely to be a viable crystal engineering strategy to design new switching CNs from first principles.

Subnetwork displacement is a phenomenon restricted to CNs that comprise individual subnets that interact with each other by weak forces, *e.g.* hydrogen bonding or van der Waals interactions. This includes interpenetrated net sliding as well as layered net expansion in 3D and 2D switching CNs, respectively. Interpenetrated net sliding usually occurs between centered interpenetrated nets (closed phase) and offset interpenetrated nets (open phase), thereby creating voids to accommodate guest molecules as exemplified by 2-fold interpenetrated PLCNs such as the X-pcu-*n*-Zn family.^{146,147} Layered net expansion occurs in 2D switching CNs thanks to their ability to offer clay-like intercalation of guest molecules as observed in switching sql CNs.^{144,145}

A question that remains to be answered is why do isostructural CNs exhibit very different structural flexibility and sorption behaviour, *e.g.* MIL-47 does not exhibit breathing behaviour whereas MIL-53 does?^{214,215} Addressing this matter requires a quantitative understanding of the energy landscape including the energy barriers between multiple phases and the energy derived from host-guest and guest-guest interactions.²¹⁶⁻²¹⁸ In addition, kinetic factors such as linker rotation dynamics can affect the framework transition, especially across transient phases.²¹⁹ In many cases, the precise mechanisms of phase transformations are beyond the scope of SCXRD, which only provides the static perspective of crystal structures. Further mechanistic insight will likely come through *in situ* experiments coupled with molecular modeling studies.



4. Applications

4.1. Gas storage

Gas storage is one of the most important and well-studied properties of porous CNs.^{220–223} Indeed, we are in the “*age of gas*”²²⁴ and physisorption is recognised as an energy-efficient approach to mitigate the energy footprint associated with traditional compression and liquefaction-based technologies. A variety of gases such as non-polar gases (H₂, O₂, N₂, Ar, Xe), polar gases (CO, NO, CO₂) and C₂–C₄ light hydrocarbon gases and vapours have been investigated in rigid porous CNs.^{220–223} 77 K N₂ sorption serves as the most common characterisation tool to experimentally determine the porosity of an adsorbent. The greenhouse gas CO₂ is another extensively studied gas at low (e.g. 195 K and 1 bar) and high (e.g. 298 K and 50 bar) temperatures and pressures, driven by the importance of carbon capture from flue gases (bulk) and air (trace). On the other hand, as a relatively inexpensive and clean fuel gas, CH₄ is of particular interest and importance given the energy footprints and limitations of liquified and compressed nature gas storage.

Recent studies have demonstrated that switching nonporous CNs that exhibit type F-IV isotherms can enable higher working capacities than physisorbents with type I isotherms as explained above (Fig. 2f). There are several other potential advantages of switching CNs for gas storage. First, since type F-IV isotherms usually exhibit hysteresis between their adsorption and desorption branches, it allows for a gas to be adsorbed at high pressure and stored at relatively low pressure.⁷² Second, switching pressure and temperature follow the Clausius–Clapeyron equation,^{72,86,144} which means that switching pressure can be calculated for a given temperature. This enables the selection of a bespoke sorbent that offers optimised parameters for temperature or pressure swing adsorption processes or combinations thereof. Last, but not least, endothermal/exothermal structural expansion/contraction in switching CNs naturally offsets the exothermal/endothermal nature of adsorption/desorption processes, thereby facilitating improved thermal management.^{74,87}

As detailed earlier herein, various gases have been studied to determine if they can induce switching in CNs (Table 1). 77 K N₂ and 195 K CO₂ sorption isotherms are well documented as summarised in Table 5. Thus far, around 20 switching CNs exhibit >100 cm³ g⁻¹ CO₂ or N₂ uptake at cryogenic temperatures and their switching pressures vary from *ca.* 0.1 to 80 kPa (Fig. 22a and b). DUT-8(Ni) exhibits the highest N₂ (670 cm³ g⁻¹) and CO₂ (590 cm³ g⁻¹) uptakes yet reported at 77 and 195 K, respectively.¹¹⁴ However, at 298 K, DUT-8(Ni) adsorbs negligible N₂ and only 58% of its saturation CO₂ uptake (345 cm³ g⁻¹) at 50 bar. For CH₄, DUT-8(Ni) was found to exhibit a characteristic type I isotherm and adsorbed only 70 cm³ g⁻¹ at 50 bar, 298 K. Other switching CNs such as X-pcu-*n*-Zn, ELM-11 and M(bdp) exhibit >200 cm³ g⁻¹ uptakes at cryogenic temperatures. With respect to the X-pcu-*n*-Zn family (*n* = 5, 6, 7, 8), X-pcu-6-Zn exhibits the lowest switching pressures for N₂ and CO₂.¹⁴⁷ At 298 K, X-pcu-*n*-Zn CNs exhibit negligible CO₂ uptake except for the “softest” variant, X-pcu-6-Zn, which adsorbs 50 cm³ g⁻¹ of CO₂ at 33 bar. Unsurprisingly, like DUT-8(Ni), high pressure CH₄ adsorption isotherms to 50 bar revealed negligible uptake for all four X-pcu-*n*-Zn CNs. ELM-11 exhibits a type F-IV^s isotherm for N₂ at 77 K and a type F-IV^m isotherm for CO₂ at 195 K with almost



Table 5 N₂ (77 K, 1 bar), CO₂ (195 K, 1 bar) and CH₄ (298 K) sorption parameters for representative switching CNs^a

CNs	N ₂ 77 K		CO ₂ 195 K		CH ₄ 298 K		Ref.
	P _{ga} (kPa)	Uptake (cm ³ g ⁻¹)	P _{ga} (kPa)	Uptake (cm ³ g ⁻¹)	P _{ga} (bar) g ⁻¹)		
DUT-8(Ni)	13	670	35	590	Type I	70	114
Co(bdp)	3	668	N.A.	N.A.	15	246	74
Fe(bdp)	0.8	638	N.A.	N.A.	25	291	
Co(F-bdp)	4	582	N.A.	N.A.	Type F-III	173	133
Co(<i>o</i> -F ₂ -bdp)	4	560	N.A.	N.A.	12	160	
Co(<i>p</i> -F ₂ -bdp)	1	504	N.A.	N.A.	10	157	
Cu(HIsa-az-dmpz)	3	360	8	310	N.A.	N.A.	150
JLU-Liu3	41	325	26 (F-II)	337	Negligible uptake till 1 bar		129
JLU-Liu4	26	306	16 (F-II)	333			
JLU-Liu33	6	319	4 (F-II)	205			135
X-dia-1-Ni	Remain closed		Type F-II	325	20	225	67
X-pcu-5-Zn	45	135	30	254	Remain closed phase up to 50 bar		146 and 147
X-pcu-6-Zn	20	290	17	245			
X-pcu-7-Zn	68	217	33	267			
X-pcu-8-Zn	Remain closed		39	243			
ELM-11	10	250	30	245	38	84	59 and 86
ELM-13	20	237	50	180	N.A.	N.A.	153
CPM-325	26	216	2.6	200	N.A.	N.A.	141
[Cu ₂ (bdc) ₂ (bpy)]	0.07	170	7	156	9	79	51 and 93
SIFSIX-23-Cu	19	160	3.7	216	N.A.	N.A.	151
Cd(bpndc)(bpy)	55	150	N.A.	N.A.	N.A.	N.A.	66
[Zn ₂ (tdc) ₂ (pvq)]	15	140	N.A.	N.A.	N.A.	N.A.	143
MIL-53(Sc)	Remain closed		75	285	N.A.	N.A.	123
Zn ₂ (tp) ₂ (dfpb)	Remain closed		40	248	N.A.	N.A.	120
Cu(OTf) ₂ (bpp) ₂	Remain closed		60	153	N.A.	N.A.	125
sql-1-Co-NCS	Remain closed		10	136	N.A.	N.A.	144
Zn(GA) ₂	Remain closed		5	132	N.A.	N.A.	111
Cd(mida) ₂	N.A.	N.A.	35	130	N.A.	N.A.	142
SNU-M11	Remain closed		18	124	N.A.	N.A.	105
f-MOF-1b	Remain closed		45	107	N.A.	N.A.	132
Cu(pyrdc)(bpp)	Remain closed		23	100	N.A.	N.A.	96
MIL-53(Fe)	N.A.	N.A.	5	95	10	56	106 and 107
Cu(dhbc) ₂ (bpy)	N.A.	N.A.	N.A.	N.A.	9	62	65

^a N.A. = not available; P_{ga} = gate adsorption pressure.

identical saturation uptakes (*ca.* 250 cm³ g⁻¹).^{59,86,87} High pressure CO₂ sorption conducted upon ELM-11 at room temperature produces the type F-IV^m isotherm but with slightly lower uptakes.⁸⁶ High pressure CH₄ sorption on ELM-11 at 303 K revealed a type F-IV^s isotherm with 84 cm³ g⁻¹ uptake,⁵⁹ close to the CO₂ uptake



registered at the first step. This adsorbed volume is comparable to that of active carbon fiber (ACF), but the recovery percentage (*i.e.*, working capacity) of ELM-11 is much higher,⁵⁹ thanks to its isotherm profile. Very recently, ELM-11 (ref. 72) and another switching PLCN, MOF-508,²²⁵ were studied for a different fuel gas storage application, the storage of the explosive gas acetylene, C₂H₂, at ambient temperature. ELM-11 exhibits a four-step type F-IVth isotherm and it can deliver 163 cm³ g⁻¹ or 174 cm³ cm⁻³ of C₂H₂ between the second and third steps. However, the switching pressure at the third step is higher than 2 bar, beyond the safety pressure limit for pure C₂H₂. It is reasonable to assume that the inclusion and intercalation of C₂H₂ into ELM-11 will desensitize C₂H₂ but this matter must be verified or a porous monolith might be exploited. In the case of the MOF-508 series, a C₂H₂ working capacity of 106 cm³ cm⁻³ can be delivered under a relatively narrow pressure range (70–120 kPa). Compared to the benchmark rigid CNs which are more suited for C₂H₂ sequestration rather than C₂H₂ storage/delivery,⁷² these two reports underline the high upside potential of switching CNs for practical C₂H₂ storage.

The switching pressure, one of the two most critical parameters for utility in the context of gas storage, is strongly affected by temperature. For example, the CO₂ switching pressure for sql-1-Co-NCS at 195 K is 0.1 bar but it increases to 26.7 bar at 298 K.¹⁴⁴ The multi-step switching nature of ELM-11 was overlooked for some time until low-temperature or high-pressure gas sorption isotherms were collected.^{72,86} Although the switching pressure for a given adsorbate can be accurately calculated using the Clausius–Clapeyron equation, once the phase transformation enthalpy is determined, it is difficult to predict the switching pressure across a range of adsorbates. For instance, it is a challenge to quantitatively predict the CH₄ switching pressure even if we know the N₂ and/or CO₂ switching pressures of a given CN. Thus far, most switching CNs that exhibit high N₂ and/or CO₂ uptake at low (*e.g.* cryogenic) temperatures exhibit low or negligible CH₄ uptake at higher temperatures and pressures. This is likely because CH₄ tends to form relatively weak interactions with most CNs, especially compared to CO₂. The switching pressure of CH₄ is expected to be much higher than that of N₂ or CO₂ at the same conditions and usually falls beyond the measurement limits of most studies reported in the literature.

With respect to methane storage, there are currently <10 switching CNs with CH₄ uptake measured at 298 K and only three (Co(bdp), Fe(bdp) and X-dia-1-Ni) exhibit >200 cm³ g⁻¹ CH₄ uptake (Fig. 22c).^{67,74} Considering its relevance to adsorbed natural gas (ANG) storage,^{226–233} the working capacity is typically determined as the quantity of NG that is deliverable between 5–35 or 5–65 bar, pressure ranges that are relevant for commercial combustion engines. In this context, Co(bdp) and Fe(bdp) would be expected to deliver around 100% of the stored NG thanks to their type F-IV isotherms.⁷⁴ To put this in context, rigid CNs that exhibit benchmark gravimetric uptake (*e.g.* >500 cm³ g⁻¹) tend to have much lower volumetric working capacities because of their relatively low densities (*e.g.* <0.3 g cm⁻³).²³³ Overall, Co(bdp) and Fe(bdp) exhibit comparable or superior volumetric working capacities (~200 cm³ cm⁻³) compared to the benchmark rigid CNs (Fig. 22d), and meet the early DOE (U.S. Department of Energy) target for volumetric CH₄ uptake (180 cm³ cm⁻³). Unfortunately, these working capacities remain well below the current DOE target of 263 cm³ cm⁻³ (350 cm³ cm⁻³ considering *ca.* 25% packing loss).²³⁴ Indeed, regardless of structural rigidity or



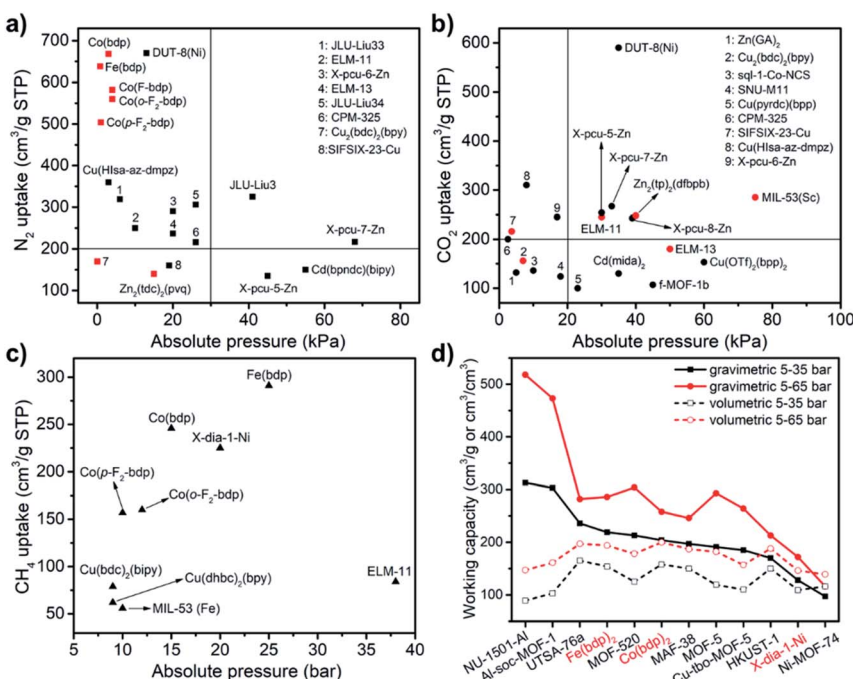


Fig. 22 Comparison of switching CNs with respect to (a) N₂ (77 K), (b) CO₂ (195 K) and (c) CH₄ (298/303 K) sorption. Black and red symbols denote CNs with type F-IV^s and F-IV^m isotherms respectively. For type F-IV^m isotherms, only the switching pressures of the last step are shown. (d) Comparison of gravimetric and volumetric working capacities for CH₄ at 298 K between current benchmarks for switching and rigid CNs.

flexibility, there is no adsorbent that yet meets the ambitious target for methane storage. Accordingly, development of new switching CNs with improved uptakes, the right switching pressures and proper densities is needed to properly exploit their intrinsically advantageous isotherms.

4.2. Separations

Separations are of industrial relevance since most commodities are obtained as mixtures and require further purification steps prior to downstream processing and utilisation.²³⁵⁻²⁴¹ Unfortunately, the energy footprint of separation/purification is generally high and currently represents ~15% of the global energy consumption because of our reliance upon energy-intensive separation methods such as distillation, evaporation, chemisorption, and crystallization.²⁴² Given that a three-fold increase in demand for commodities is projected to occur by 2050,²²⁴ more energy-efficient purification technologies are urgently required. In this context, adsorptive separation using porous solids is increasingly recognised as a promising alternative to traditional methods. Purification of a wide range of mixtures, from gaseous (e.g. CH₄/CO₂, CH₄/N₂, C₂H₂/CO₂, C₂H₂/C₂H₄/C₂H₆, C₃H₄/C₃H₆/C₃H₈) to vapour and liquid forms (e.g. C₅, C₆ alkanes and C₇, C₈ aromatics) have been extensively studied using rigid porous CNs.²³⁵⁻²⁴¹



Switching CNs	Mixtures	Separation performance	Methods	Conditions	Ref.
ELM-11	CO_2/CH_4	$S_{\text{CO}_2/\text{CH}_4}$: 31 $S_{\text{CO}_2/\text{CH}_4}$: 66.7 CH_4/N_2 $S_{\text{CH}_4/\text{N}_2}$: 8.7	BT (50 : 50)	298 K, 20 bar 273 K, 1 bar 195 K, 20 bar	128
Cu(dhbc) ₂ (bpy)	CO_2/CH_4	$S_{\text{CO}_2/\text{CH}_4}$: 28.9 $S_{\text{CO}_2/\text{CH}_4}$: 53.4 CH_4/N_2 $S_{\text{CH}_4/\text{N}_2}$: 5.5 $S_{\text{CH}_4/\text{N}_2}$: 10.3		298 K, 10 bar 273 K, 1 bar 273 K, 20 bar 195 K, 1 bar	
ELM-11	$\text{C}_2\text{H}_2/$ C_2H_4	$S_{\text{CO}_2/\text{CH}_4}$: 10^8 to 10^9 $S_{\text{CO}_2/\text{CH}_4}$: 10–100 C_2H_2 preference	IAST (50 : 50) IAST (10 : 90) BT (50 : 50) BT (10 : 90)	298 K, 1 bar	85
ELM-13		$S_{\text{CO}_2/\text{CH}_4}$: 10^4 to 10^5 $S_{\text{CO}_2/\text{CH}_4}$: 10^4 to 10^5 C_2H_2 preference	IAST (50 : 50) IAST (10 : 90) BT (50 : 50) BT (10 : 90)		
Co(bdp)	CO_2/CH_4	Near-perfect selectivity (exact values not given)	BEA (46 : 54) BEA (42 : 58) BEA (43 : 57)	298 K, 6.7 bar 298 K, 13.9 bar 298 K, 25.3 bar	103
NJU-Bai8	$\text{C}_3\text{H}_6/$ C_3H_8	$S_{\text{CO}_2/\text{CH}_4}$: 61 $S_{\text{C}_3\text{O}_6/\text{C}_3\text{H}_8}$: 4.6 C_3H_6 preference	IAST (50 : 50) BT (20 : 20)	298 K, 58.6 bar 298 K, 20 kPa 298 K, 1 bar	78
NTU-65 (SIFSIX-23-Cu)	$\text{C}_2\text{H}_2/$ C_2H_4 $\text{CO}_2/\text{C}_2\text{H}_4$ $\text{C}_2\text{H}_2/$ $\text{CO}_2/\text{C}_2\text{H}_4$	Outlet >99.95% C_2H_4	BT (1 : 99)	263 K, 1 bar	152
Co(VTTE) ₂	$\text{C}_2\text{H}_4/$ C_2H_6	$S_{\text{C}_2\text{H}_4/\text{C}_2\text{H}_6}$: 5.1 $S_{\text{C}_2\text{H}_4/\text{C}_2\text{H}_6}$: 1.9	BEA (10 : 90) BEA (50 : 50)	190 K, 1 bar	70
ELM-13	CO_2/N_2	$S_{\text{CO}_2/\text{N}_2}$: 13.3	BEA (50 : 50)	273 K, 10 bar	82
sql-1-Co-NCS	OX/MX OX/PX MX/PX OX/EB MX/EB PX/EB	$S_{\text{OX}/\text{MX}}$: 7.5 $S_{\text{OX}/\text{PX}}$: 9.6 $S_{\text{MX}/\text{PX}}$: 1.3 $S_{\text{OX}/\text{EB}}$: 60.1 $S_{\text{MX}/\text{EB}}$: 3.8 $S_{\text{PX}/\text{EB}}$: 7.3	BEA (1 : 1)	Room temperature, liquid phase	145
MIL-53(Fe)	OX/MX OX/PX MX/PX	$S_{\text{OX}/\text{MX}}$: 2.66 $S_{\text{OX}/\text{PX}}$: 1.88 $S_{\text{OX}/\text{MX}}$: 1.51	BT (1 : 1)	323 K, 0.05 M in heptane	175
DynaMOF-100	OX/PX/ MX/EB ST/EB	PX preference $S_{\text{OX}/\text{PX}}$: 1.51 ST preference	QEA (1 : 1 : 1 : 1)	Room temperature, liquid phase	60
			BEA (1 : 1)		

^a BT: breakthrough; IAST: ideal adsorbed solution theory; BEA (QEA): binary (quaternary) equilibrium adsorption.



Switching nonporous CNs remain underexplored in the context of separation but they are attracting increasing attention as stepwise adsorption can endow switching CNs with high adsorption selectivities, at least in principle (*e.g.* based on Henry's law and/or IAST calculations). This is especially the case when a single component of a mixture exclusively induces structural transformation(s). However, in practice, separation performances tend to be inferior to the theoretical values derived from pure-component sorption isotherms. This is because of the complexities of dynamic conditions, especially sorption/diffusion kinetics and coadsorption. Switching CNs might also be unsuited for trace gas removal (*e.g.* <1000 ppm, or 0.1%) because the switching pressure is normally well above 0.1 kPa at room temperature. Nevertheless, switching CNs hold promise for adsorptive separation as reflected in some of the benchmark separation performances registered in Table 6. For example, ELM-11 exhibits good selectivity for CO₂ over CH₄ (66.7) at 273 K and 1 bar as verified by breakthrough experiments.²⁴³ Importantly, ELM-11 also retains this CO₂/CH₄ separation performance at 298 K and 20 bar, making it favourable for separation of a CH₄/CO₂ stream obtained directly from a natural gas source. Similarly, high-pressure purification of CH₄ is also observed in Co(bdp), which exhibits "near-perfect" selectivity of CO₂ over CH₄ as confirmed by binary equilibrium adsorption experiments.¹⁰³ Another **sql** CN, sql-1-Co-NCS, was found to exhibit excellent separation performance towards C₈ aromatic isomers,¹⁴⁵ one of the seven separation challenges that could "*change the world*".²⁴² This switching adsorbent layered material (SALMA) is the first sorbent that combines high xylene uptake (>50 wt%) with high selectivity (>5).¹⁴⁵ MIL-53(Fe) also exhibited potential to separate xylene isomers,¹⁷⁷ but its selectivity was determined to be lower than those of sql-1-Co-NCS and MIL-53(Al).^{145,244,245} Another recent example of a high performing switching CN is NTU-65 (also termed SIFSIX-23-Cu).¹⁵² Compared to zeolites and rigid CNs, NTU-65 exhibited comparable or superior separation performance for C₂H₄ purification from C₂H₂ and CO₂ impurities. In summary, there is much scope to further explore the separation properties and performance of switching CNs which already show, perhaps counterintuitively, great promise for several separations that have been a great challenge for rigid physisorbents.

Apart from working capacity and selectivity as discussed above, recyclability and kinetics are two other key metrics that must be evaluated for practical application, yet both remain largely understudied. Despite the strong recyclability demonstrated by Co(bdp)⁷⁴ and X-pcu-*n*-Zn,^{146,147} several 3D switching CNs, such as X-dia-1-Ni,⁶⁷ DUT-8(Ni)²⁴⁶ and [Zn₂(DPT)₂(bpy)]¹³⁶ suffered from degradation in terms of switching pressure and uptake after multiple gas sorption cycles. In contrast, 2D layered switching CNs such as ELM-11 (ref. 246) and sql-1-Co-NCS¹⁴⁴ demonstrated excellent recyclability over at least 100 cycles. The strong recyclability performance of several 2D CNs might be attributed to the relatively low structural strain and/or weak inter-network interactions that accompany expansion/contraction during recycling. With respect to kinetics, the CH₄ adsorption kinetics of ELM-11 reached saturation uptake in 10 min (ref. 59) and we demonstrated that the CO₂ adsorption of sql-1-Co-NCS requires less than 30 min.¹⁴⁴ In general, the adsorption kinetics of switching CNs is even less well-studied than recyclability.



5. Conclusions

We detail herein the scope of CNs that switch between closed and open phases, an emerging class of physisorbents, and discuss the impact of metal ions, linker ligands and adsorbates on switching parameters upon properties of relevance to gas storage and separations. We also address the mechanisms associated with switching between closed and open phases. Switching CNs offer potential advantages over rigid CNs which results from their extreme flexibility, the specific stimulus-response and unusual sorption properties. However, both scientific and practical hurdles remain to be overcome before there can be utility.

From a scientific perspective, the synthetic design principles for switching or, more generally, even soft CNs largely remain to be established. This is despite the relative maturity of crystal engineering with respect to design of CNs from first principles. The introduction of switching elements into CNs and realisation of structural dynamism remains somewhat unpredictable due to uncertainties over their self-assembly processes and the complex interplay of local and global flexibility. Indeed, as revealed by Table 5, other than the effect of temperature and pressure upon switching pressure, there is no obvious correlation between sorbates and switching pressure other than the general observation that polar sorbates tend to promote switching. Improvements in understanding and predictability of switching will come from in-depth investigation of the origin and mechanism of switching, which remains limited by a reliance on X-ray diffraction.²⁴⁷ It is therefore important to further exploit *in situ* characterization using techniques such as nuclear magnetic resonance, Raman spectroscopy, transmission electron microscopy and neutron scattering to broaden the scopes offered by diffraction experiments.⁴⁵ In this context, given the dynamics of switching transformations, time-resolved *in situ* techniques are of particular importance.^{176,248} It is also worth mentioning that the performance of CNs is determined not only by their atomic level structure, but also by their macroscopic features, *i.e.*, morphology, particle size, *etc*. Therefore, further insights into the roles of particle size, morphology, defects and disorder are needed.^{249–251} Finally, development of machine learning and task-specific theoretical modelling approaches merit increased attention since they might not only address the underlying mechanisms, but also offer predictable modelling of the performance of switching CNs with pre-defined functions.^{252–254}

From a practical viewpoint, the hygroscopicity of CNs must be taken into account in addition to the aforementioned performance metrics (*i.e.*, recyclability and kinetics). This is because hygroscopicity can strongly impact both the lifetime and the performance of switching CNs.²⁵⁵ In addition, that switching between closed and open phases usually results in large volume changes in switching CNs may pose challenges to downstream processes such as formulation/shaping. It should be noted that the activation can also influence the switching pressure and uptake.^{28,136} Cost of ingredients and processing is also a consideration that must be addressed when assessing the viability of CN-based products and technologies. Ironically, even though this is not considered by most academic researchers, this is perhaps the one factor that a chemist can control. With respect to processing, the use of mechanochemistry such as ball milling and twin-screw extrusion²⁵⁶ offers promise for scale-up and several well-known rigid CNs have been prepared

with high efficiency using mechanochemistry.²⁵⁷ The suitability of mechanochemistry for synthesis of switching or soft CNs is even more understudied though.

In conclusion, we are perhaps approaching the “end of the beginning”, but we are not yet there in terms of either design or properties. With respect to design, there are still just a few families of switching CNs and we remain mainly at the stage of empirical observation. With respect to properties, apart from adsorptive gas storage and mixture separation as discussed above, switching CNs and derived composites have been noted as having the potential to serve other emerging applications thanks to combination(s) of different applied stimuli such as light, redox and mechanical stress.^{258–261} Whereas these applications emphasise the relevance of switching CNs more than ever, there remains a large gap between a property serving as an indicator of performance and real-world applications. At this stage, ANG storage is perhaps the most promising short to medium term opportunity for end-use of switching CNs.

Conflicts of interest

There are no conflicts to declare.

Acknowledgements

M. J. Z. would like to acknowledge the support of Irish Research Council (IRCLA/2019/167) and Science Foundation Ireland (13/RP/B2549 and 16/IA/4624). S. M. thanks the Alexander von Humboldt Foundation for funding his postdoctoral research at TU Munich. S.-Q. W. would like to thank his colleague Dr Shaza Darwish for her proof reading and helpful suggestions.

References

- 1 S. R. Batten, N. R. Champness, X.-M. Chen, J. Garcia-Martinez, S. Kitagawa, L. Öhrström, M. O’Keeffe, M. P. Suh and J. Reedijk, *Pure Appl. Chem.*, 2013, **85**, 1715–1724.
- 2 L. R. MacGillivray, *Metal–organic frameworks: design and application*, Wiley, Hoboken, 2010.
- 3 D. Farrusseng, *Metal–Organic Frameworks: Applications from Catalysis to Gas Storage*, Wiley-VCH, Weinheim, 2011.
- 4 J. F. Keggin and F. D. Miles, *Nature*, 1936, **137**, 577–578.
- 5 H. J. Buser, D. Schwarzenbach, W. Petter and A. Ludi, *Inorg. Chem.*, 1977, **16**, 2704–2710.
- 6 S. Mukherjee and M. J. Zaworotko, *Trends Chem.*, 2020, **2**, 506–518.
- 7 S. Kitagawa, R. Kitaura and S.-i. Noro, *Angew. Chem., Int. Ed.*, 2004, **43**, 2334–2375.
- 8 S. R. Batten, S. M. Neville and D. R. Turner, *Coordination Polymers: Design, Analysis and Application*, Royal Society of Chemistry, London, 2009.
- 9 J. J. Perry IV, J. A. Perman and M. J. Zaworotko, *Chem. Soc. Rev.*, 2009, **38**, 1400–1417.
- 10 T. R. Cook, Y.-R. Zheng and P. J. Stang, *Chem. Rev.*, 2013, **113**, 734–777.
- 11 B. Moulton and M. J. Zaworotko, *Chem. Rev.*, 2001, **101**, 1629–1658.

12 O. M. Yaghi, M. O'Keeffe, N. W. Ockwig, H. K. Chae, M. Eddaoudi and J. Kim, *Nature*, 2003, **423**, 705–714.

13 B. F. Hoskins and R. Robson, *J. Am. Chem. Soc.*, 1989, **111**, 5962–5964.

14 B. F. Hoskins and R. Robson, *J. Am. Chem. Soc.*, 1990, **112**, 1546–1554.

15 S. Ma and H.-C. Zhou, *Chem. Commun.*, 2010, **46**, 44–53.

16 J.-R. Li, J. Sculley and H.-C. Zhou, *Chem. Rev.*, 2012, **112**, 869–932.

17 P. A. Kobielska, A. J. Howarth, O. K. Farha and S. Nayak, *Coord. Chem. Rev.*, 2018, **358**, 92–107.

18 P. Horcajada, R. Gref, T. Baati, P. K. Allan, G. Maurin, P. Couvreur, G. Férey, R. E. Morris and C. Serre, *Chem. Rev.*, 2012, **112**, 1232–1268.

19 J. Y. Lee, O. K. Farha, J. Roberts, K. A. Scheidt, S. B. T. Nguyen and J. T. Hupp, *Chem. Soc. Rev.*, 2009, **38**, 1450–1459.

20 P. Z. Moghadam, A. Li, X.-W. Liu, R. Bueno-Perez, S.-D. Wang, S. B. Wiggin, P. A. Wood and D. Fairen-Jimenez, *Chem. Sci.*, 2020, **11**, 8373–8387.

21 R. Taylor and P. A. Wood, *Chem. Rev.*, 2019, **119**, 9427–9477.

22 S. Kitagawa and M. Kondo, *Bull. Chem. Soc. Jpn.*, 1998, **71**, 1739–1753.

23 K. Uemura, R. Matsuda and S. Kitagawa, *J. Solid State Chem.*, 2005, **178**, 2420–2429.

24 S. Kitagawa and K. Uemura, *Chem. Soc. Rev.*, 2005, **34**, 109–119.

25 G. Alberti, S. Murcia-Mascaros and R. Vivani, *J. Am. Chem. Soc.*, 1998, **120**, 9291–9295.

26 G. Alberti, E. Brunet, C. Dionigi, O. Juanes, M. J. de la Mata, J. C. Rodríguez-Ubis and R. Vivani, *Angew. Chem., Int. Ed.*, 1999, **38**, 3351–3353.

27 O.-S. Jung, Y. J. Kim, Y.-A. Lee, J. K. Park and H. K. Chae, *J. Am. Chem. Soc.*, 2000, **122**, 9921–9925.

28 D. Li and K. Kaneko, *Chem. Phys. Lett.*, 2001, **335**, 50–56.

29 A. J. Fletcher, E. J. Cussen, T. J. Prior, M. J. Rosseinsky, C. J. Kepert and K. M. Thomas, *J. Am. Chem. Soc.*, 2001, **123**, 10001–10011.

30 S. Horike, S. Shimomura and S. Kitagawa, *Nat. Chem.*, 2009, **1**, 695–704.

31 S. Krause, N. Hosono and S. Kitagawa, *Angew. Chem., Int. Ed.*, 2020, **59**, 15325–15341.

32 S. Castellanos, F. Kapteijn and J. Gascon, *CrystEngComm*, 2016, **18**, 4006–4012.

33 H.-L. Zhou, Y.-B. Zhang, J.-P. Zhang and X.-M. Chen, *Nat. Commun.*, 2015, **6**, 1–7.

34 I. Beurroies, M. Boulhout, P. L. Llewellyn, B. Kuchta, G. Férey, C. Serre and R. Denoyel, *Angew. Chem., Int. Ed.*, 2010, **49**, 7526–7529.

35 M.-H. Yu, B. Space, D. Franz, W. Zhou, C. He, L. Li, R. Krishna, Z. Chang, W. Li, T.-L. Hu and X.-H. Bu, *J. Am. Chem. Soc.*, 2019, **141**, 17703–17712.

36 H. Zeng, M. Xie, Y.-L. Huang, Y. Zhao, X.-J. Xie, J.-P. Bai, M.-Y. Wan, R. Krishna, W. Lu and D. Li, *Angew. Chem., Int. Ed.*, 2019, **58**, 8515–8519.

37 P. Zhao, H. Fang, S. Mukhopadhyay, A. Li, S. Rudic, I. J. McPherson, C. C. Tang, D. Fairen-Jimenez, S. C. E. Tsang and S. A. T. Redfern, *Nat. Commun.*, 2019, **10**, 1–8.

38 G. Férey and C. Serre, *Chem. Soc. Rev.*, 2009, **38**, 1380–1399.

39 A. J. Fletcher, K. M. Thomas and M. J. Rosseinsky, *J. Solid State Chem.*, 2005, **178**, 2491–2510.

40 C. R. Murdock, B. C. Hughes, Z. Lu and D. M. Jenkins, *Coord. Chem. Rev.*, 2014, **258**, 119–136.



41 A. Schneemann, V. Bon, I. Schwedler, I. Senkovska, S. Kaskel and R. A. Fischer, *Chem. Soc. Rev.*, 2014, **43**, 6062–6096.

42 B. Qian, Z. Chang and X.-H. Bu, *Top. Curr. Chem.*, 2020, **378**, 5.

43 F. Bigdeli, C. T. Lollar, A. Morsali and H.-C. Zhou, *Angew. Chem., Int. Ed.*, 2020, **59**, 4652–4669.

44 S. B. Peh, A. Karmakar and D. Zhao, *Trends Chem.*, 2020, **2**, 199–213.

45 V. Bon, E. Brunner, A. Pöppl and S. Kaskel, *Adv. Funct. Mater.*, 2020, **30**, 1907847.

46 J.-P. Zhang, H.-L. Zhou, D.-D. Zhou, P.-Q. Liao and X.-M. Chen, *Natl. Sci. Rev.*, 2018, **5**, 907–919.

47 L. Vanduyfhuys, S. Rogge, J. Wieme, S. Vandenbrande, G. Maurin, M. Waroquier and V. Van Speybroeck, *Nat. Commun.*, 2018, **9**, 1–9.

48 Z. Chang, D.-H. Yang, J. Xu, T.-L. Hu and X.-H. Bu, *Adv. Mater.*, 2015, **27**, 5432–5441.

49 S. K. Elsaiedi, M. H. Mohamed, D. Banerjee and P. K. Thallapally, *Coord. Chem. Rev.*, 2018, **358**, 125–152.

50 J. H. Lee, S. Jeoung, Y. G. Chung and H. R. Moon, *Coord. Chem. Rev.*, 2019, **389**, 161–188.

51 K. Seki, *Phys. Chem. Chem. Phys.*, 2002, **4**, 1968–1971.

52 K. Biradha and M. Fujita, *Angew. Chem., Int. Ed.*, 2002, **41**, 3392–3395.

53 J.-S. Qin, S. Yuan, A. Alsalme and H.-C. Zhou, *ACS Appl. Mater. Interfaces*, 2017, **9**, 33408–33412.

54 Q.-f. Qiu, C.-X. Chen, Z.-W. Wei, C.-C. Cao, N.-X. Zhu, H.-P. Wang, D. Wang, J.-J. Jiang and C.-Y. Su, *Inorg. Chem.*, 2019, **58**, 61–64.

55 C. Serre, F. Millange, C. Thouvenot, M. Nogues, G. Marsolier, D. Louër and G. Férey, *J. Am. Chem. Soc.*, 2002, **124**, 13519–13526.

56 C. Mellot-Draznieks, C. Serre, S. Surblé, N. Audebrand and G. Férey, *J. Am. Chem. Soc.*, 2005, **127**, 16273–16278.

57 C. Serre, C. Mellot-Draznieks, S. Surblé, N. Audebrand, Y. Filinchuk and G. Férey, *Science*, 2007, **315**, 1828–1831.

58 A. U. Ortiz, A. Boutin, A. H. Fuchs and F.-X. Coudert, *Phys. Rev. Lett.*, 2012, **109**, 195502.

59 H. Kanoh, A. Kondo, H. Noguchi, H. Kajiro, A. Tohdoh, Y. Hattori, W.-C. Xu, M. Inoue, T. Sugiura, K. Morita, H. Tanaka, T. Ohba and K. Kaneko, *J. Colloid Interface Sci.*, 2009, **334**, 1–7.

60 K. Yang, G. Zhou and Q. Xu, *RSC Adv.*, 2016, **6**, 37506–37514.

61 H. Deng, M. A. Olson, J. F. Stoddart and O. M. Yaghi, *Nat. Chem.*, 2010, **2**, 439–443.

62 A. Gonzalez-Nelson, F.-X. Coudert and M. A. van der Veen, *Nanomaterials*, 2019, **9**, 330.

63 S. Krause, V. Bon, U. Stoeck, I. Senkovska, D. M. Toebbens, D. Wallacher and S. Kaskel, *Angew. Chem., Int. Ed.*, 2017, **56**, 10676–10680.

64 P. Kanoo, R. Haldar, S. K. Reddy, A. Hazra, S. Bonakala, R. Matsuda, S. Kitagawa, S. Balasubramanian and T. K. Maji, *Chem.-Eur. J.*, 2016, **22**, 15864–15873.

65 R. Kitaura, K. Seki, G. Akiyama and S. Kitagawa, *Angew. Chem., Int. Ed.*, 2003, **42**, 428–431.

66 D. Tanaka, K. Nakagawa, M. Higuchi, S. Horike, Y. Kubota, T. C. Kobayashi, M. Takata and S. Kitagawa, *Angew. Chem., Int. Ed.*, 2008, **47**, 3914–3918.



67 Q. Y. Yang, P. Lama, S. Sen, M. Lusi, K. J. Chen, W. Y. Gao, M. Shivanna, T. Pham, N. Hosono, S. Kusaka, J. J. Perry IV, S. Ma, B. Space, L. J. Barbour, S. Kitagawa and M. J. Zaworotko, *Angew. Chem., Int. Ed.*, 2018, **57**, 5684–5689.

68 M. Thommes, K. Kaneko, A. V. Neimark, J. P. Olivier, F. Rodriguez-Reinoso, J. Rouquerol and K. S. Sing, *Pure Appl. Chem.*, 2015, **87**, 1051–1069.

69 S. Bourrelly, P. L. Llewellyn, C. Serre, F. Millange, T. Loiseau and G. Férey, *J. Am. Chem. Soc.*, 2005, **127**, 13519–13521.

70 A. Kondo, H. Noguchi, L. Carlucci, D. M. Proserpio, G. Ciani, H. Kajiro, T. Ohba, H. Kanoh and K. Kaneko, *J. Am. Chem. Soc.*, 2007, **129**, 12362–12363.

71 A. Schneemann, P. Vervoorts, I. Hante, M. Tu, S. Wannapaiboon, C. Sternemann, M. Paulus, D. C. F. Wieland, S. Henke and R. A. Fischer, *Chem. Mater.*, 2018, **30**, 1667–1676.

72 S.-Q. Wang, X.-Q. Meng, M. Vandichel, S. Darwish, Z. Chang, X.-H. Bu and M. J. Zaworotko, *ACS Appl. Mater. Interfaces*, 2021, **13**, 23877–23883.

73 M. Shivanna, Q.-Y. Yang, A. Bajpai, S. Sen, N. Hosono, S. Kusaka, T. Pham, K. A. Forrest, B. Space, S. Kitagawa and M. J. Zaworotko, *Sci. Adv.*, 2018, **4**, eaq1636.

74 J. A. Mason, J. Oktawiec, M. K. Taylor, M. R. Hudson, J. Rodriguez, J. E. Bachman, M. I. Gonzalez, A. Cervellino, A. Guagliardi, C. M. Brown, P. L. Llewellyn, N. Masciocchi and J. R. Long, *Nature*, 2015, **527**, 357–361.

75 E. Coronado and G. Minguez Espallargas, *Chem. Soc. Rev.*, 2013, **42**, 1525–1539.

76 S. Castellanos, F. Kapteijn and J. Gascon, *CrystEngComm*, 2016, **18**, 4006–4012.

77 O. Drath and C. Boskovic, *Coord. Chem. Rev.*, 2018, **375**, 256–266.

78 W. D. Schaeffer, W. S. Dorsey, D. A. Skinner and C. G. Christian, *J. Am. Chem. Soc.*, 1957, **79**, 5870–5876.

79 S. A. Allison and R. M. Barrer, *J. Chem. Soc. A*, 1969, 1717–1723.

80 T. Dewa, K. Endo and Y. Aoyama, *J. Am. Chem. Soc.*, 1998, **120**, 8933–8940.

81 Z. Wang, N. Sikdar, S.-Q. Wang, X. Li, M. Yu, X.-H. Bu, Z. Chang, X. Zou, Y. Chen, P. Cheng, K. Yu, M. J. Zaworotko and Z. Zhang, *J. Am. Chem. Soc.*, 2019, **141**, 9408–9414.

82 N. Sun, S.-Q. Wang, R. Zou, W.-G. Cui, A. Zhang, T. Zhang, Q. Li, Z.-Z. Zhuang, Y.-H. Zhang, J. Xu, M. J. Zaworotko and X.-H. Bu, *Chem. Sci.*, 2019, **10**, 8850–8854.

83 A. M. Kałuża, S. Mukherjee, S.-Q. Wang, D. J. O’Hearn and M. J. Zaworotko, *Chem. Commun.*, 2020, **56**, 1940–1943.

84 G. B. Gardner, D. Venkataraman, J. S. Moore and S. Lee, *Nature*, 1995, **374**, 792–795.

85 L. Li, R. Krishna, Y. Wang, X. Wang, J. Yang and J. Li, *Eur. J. Inorg. Chem.*, 2016, **2016**, 4457–4462.

86 M. Ichikawa, A. Kondo, H. Noguchi, N. Kojima, T. Ohba, H. Kajiro, Y. Hattori and H. Kanoh, *Langmuir*, 2016, **32**, 9722–9726.

87 S. Hiraide, H. Tanaka, N. Ishikawa and M. T. Miyahara, *ACS Appl. Mater. Interfaces*, 2017, **9**, 41066–41077.

88 A. Kondo, H. Noguchi, S. Ohnishi, H. Kajiro, A. Tohdoh, Y. Hattori, W.-C. Xu, H. Tanaka, H. Kanoh and K. Kaneko, *Nano Lett.*, 2006, **6**, 2581–2584.

89 H. Kajiro, A. Kondo, K. Kaneko and H. Kanoh, *Int. J. Mol. Sci.*, 2010, **11**, 3803–3845.



90 V. Bon, I. Senkovska, D. Wallacher, A. Heerwig, N. Klein, I. Zizak, R. Feyerherm, E. Dudzik and S. Kaskel, *Microporous Mesoporous Mater.*, 2014, **188**, 190–195.

91 K. Uemura, S. Kitagawa, M. Kondo, K. Fukui, R. Kitaura, H.-C. Chang and T. Mizutani, *Chem.-Eur. J.*, 2002, **8**, 3586–3600.

92 R. Kitaura, K. Fujimoto, S. i. Noro, M. Kondo and S. Kitagawa, *Angew. Chem., Int. Ed.*, 2002, **41**, 133–135.

93 Y. Sakata, S. Furukawa, M. Kondo, K. Hirai, N. Horike, Y. Takashima, H. Uehara, N. Louvain, M. Meilikov, T. Tsruoka, S. Isoda, W. Kosaka, O. Sakata and S. Kitagawa, *Science*, 2013, **339**, 193–196.

94 Y. Inubushi, S. Horike, T. Fukushima, G. Akiyama, R. Matsuda and S. Kitagawa, *Chem. Commun.*, 2010, **46**, 9229–9231.

95 K. Uemura, S. Kitagawa, K. Fukui and K. Saito, *J. Am. Chem. Soc.*, 2004, **126**, 3817–3828.

96 T. K. Maji, G. Mostafa, R. Matsuda and S. Kitagawa, *J. Am. Chem. Soc.*, 2005, **127**, 17152–17153.

97 B. Chen, C. Liang, J. Yang, D. S. Contreras, Y. L. Clancy, E. B. Lobkovsky, O. M. Yaghi and S. Dai, *Angew. Chem., Int. Ed.*, 2006, **45**, 1390–1393.

98 S. Xiang, W. Zhou, J. M. Gallegos, Y. Liu and B. Chen, *J. Am. Chem. Soc.*, 2009, **131**, 12415–12419.

99 P. M. Bhatt, E. Batisai, V. J. Smith and L. J. Barbour, *Chem. Commun.*, 2016, **52**, 11374–11377.

100 S. Shimomura, S. Horike, R. Matsuda and S. Kitagawa, *J. Am. Chem. Soc.*, 2007, **129**, 10990–10991.

101 H. J. Choi, M. Dincă and J. R. Long, *J. Am. Chem. Soc.*, 2008, **130**, 7848–7850.

102 F. Salles, G. Maurin, C. Serre, P. L. Llewellyn, C. Knofel, H. J. Choi, Y. Filinchuk, L. Oliviero, A. Vimont, J. R. Long and G. Ferey, *J. Am. Chem. Soc.*, 2010, **132**, 13782–13788.

103 M. K. Taylor, T. Runčevski, J. Oktawiec, J. E. Bachman, R. L. Siegelman, H. Jiang, J. A. Mason, J. D. Tarver and J. R. Long, *J. Am. Chem. Soc.*, 2018, **140**, 10324–10331.

104 A. Kondo, A. Chinen, H. Kajiro, T. Nakagawa, K. Kato, M. Takata, Y. Hattori, F. Okino, T. Ohba, K. Kaneko and H. Kanoh, *Chem.-Eur. J.*, 2009, **15**, 7549–7553.

105 H. S. Choi and M. P. Suh, *Angew. Chem., Int. Ed.*, 2009, **48**, 6865–6869.

106 P. L. Llewellyn, P. Horcajada, G. Maurin, T. Devic, N. Rosenbach, S. Bourrelly, C. Serre, D. Vincent, S. Loera-Serna, Y. Filinchuk and G. Ferey, *J. Am. Chem. Soc.*, 2009, **131**, 13002–13008.

107 N. Guillou, S. Bourrelly, P. L. Llewellyn, R. I. Walton and F. Millange, *CrystEngComm*, 2015, **17**, 422–429.

108 M. Agrawal, S. Bhattacharyya, Y. Huang, K. C. Jayachandrababu, C. R. Murdock, J. A. Bentley, A. Rivas-Cardona, M. M. Mertens, K. S. Walton, D. S. Sholl and S. Nair, *J. Phys. Chem. C*, 2018, **122**, 386–397.

109 J. Seo, R. Matsuda, H. Sakamoto, C. Bonneau and S. Kitagawa, *J. Am. Chem. Soc.*, 2009, **131**, 12792–12800.

110 H. Chun and J. Seo, *Inorg. Chem.*, 2009, **48**, 9980–9982.

111 J. Rabone, Y. F. Yue, S. Y. Chong, K. C. Stylianou, J. Bacsá, D. Bradshaw, G. R. Darling, N. G. Berry, Y. Z. Khimyak, A. Y. Ganin, P. Wiper, J. B. Claridge and M. J. Rosseinsky, *Science*, 2010, **329**, 1053–1057.



112 T. Fukushima, S. Horike, Y. Inubushi, K. Nakagawa, Y. Kubota, M. Takata and S. Kitagawa, *Angew. Chem., Int. Ed.*, 2010, **49**, 4820–4824.

113 N. Klein, C. Herzog, M. Sabo, I. Senkovska, J. Getzschmann, S. Paasch, M. R. Lohe, E. Brunner and S. Kaskel, *Phys. Chem. Chem. Phys.*, 2010, **12**, 11778–11784.

114 N. Klein, H. C. Hoffmann, A. Cadiau, J. Getzschmann, M. R. Lohe, S. Paasch, T. Heydenreich, K. Adil, I. Senkovska, E. Brunner and S. Kaskel, *J. Mater. Chem.*, 2012, **22**, 10303–10312.

115 V. Bon, N. Klein, I. Senkovska, A. Heerwig, J. Getzschmann, D. Wallacher, I. Zizak, M. Brzhezinskaya, U. Mueller and S. Kaskel, *Phys. Chem. Chem. Phys.*, 2015, **17**, 17471–17479.

116 N. Kavoosi, T. Savchenko, I. Senkovska, M. Maliuta, V. Bon, A. Eychmüller and S. Kaskel, *Microporous Mesoporous Mater.*, 2018, **271**, 169–174.

117 S. Ehrling, I. Senkovska, V. Bon, J. D. Evans, P. Petkov, Y. Krupskaya, V. Kataev, T. Wulf, A. Krylov, A. Vtyurin, S. Krylova, S. Adichtchev, E. Slyusareva, M. S. Weiss, B. Büchner, T. Heine and S. Kaskel, *J. Mater. Chem. A*, 2019, **7**, 21459–21475.

118 H. Wu, R. S. Reali, D. A. Smith, M. C. Trachtenberg and J. Li, *Chem.-Eur. J.*, 2010, **16**, 13951–13954.

119 N. Nijem, H. Wu, P. Canepa, A. Marti, K. J. Balkus, T. Thonhauser, J. Li and Y. J. Chabal, *J. Am. Chem. Soc.*, 2012, **134**, 15201–15204.

120 J. Seo, C. Bonneau, R. Matsuda, M. Takata and S. Kitagawa, *J. Am. Chem. Soc.*, 2011, **133**, 9005–9013.

121 S. Henke, A. Schneemann, A. Wuetscher and R. A. Fischer, *J. Am. Chem. Soc.*, 2012, **134**, 9464–9474.

122 J. P. Mowat, V. R. Seymour, J. M. Griffin, S. P. Thompson, A. M. Slawin, D. Fairen-Jimenez, T. Düren, S. E. Ashbrook and P. A. Wright, *Dalton Trans.*, 2012, **41**, 3937–3941.

123 L. Chen, J. P. S. Mowat, D. Fairen-Jimenez, C. A. Morrison, S. P. Thompson, P. A. Wright and T. Duren, *J. Am. Chem. Soc.*, 2013, **135**, 15763–15773.

124 X.-M. Liu, R.-B. Lin, J.-P. Zhang and X.-M. Chen, *Inorg. Chem.*, 2012, **51**, 5686–5692.

125 K. Fukuhara, S.-i. Noro, K. Sugimoto, T. Akutagawa, K. Kubo and T. Nakamura, *Inorg. Chem.*, 2013, **52**, 4229–4237.

126 B. Joarder, S. Mukherjee, A. K. Chaudhari, A. V. Desai, B. Manna and S. K. Ghosh, *Chem.-Eur. J.*, 2014, **20**, 15303–15308.

127 S. Mukherjee, B. Joarder, B. Manna, A. V. Desai, A. K. Chaudhari and S. K. Ghosh, *Sci. Rep.*, 2014, **4**, 5761.

128 S. Mukherjee, B. Joarder, A. V. Desai, B. Manna, R. Krishna and S. K. Ghosh, *Inorg. Chem.*, 2015, **54**, 4403–4408.

129 J. Wang, J. Luo, J. Zhao, D.-S. Li, G. Li, Q. Huo and Y. Liu, *Cryst. Growth Des.*, 2014, **14**, 2375–2380.

130 M. Handke, H. Weber, M. Lange, J. Moellmer, J. Lincke, R. Glaeser, R. Staudt and H. Krautscheid, *Inorg. Chem.*, 2014, **53**, 7599–7607.

131 C. Wang, L. Li, J. G. Bell, X. Lv, S. Tang, X. Zhao and K. M. Thomas, *Chem. Mater.*, 2015, **27**, 1502–1516.

132 P. Kanoo, R. Haldar, S. K. Reddy, A. Hazra, S. Bonakala, R. Matsuda, S. Kitagawa, S. Balasubramanian and T. K. Maji, *Chem.-Eur. J.*, 2016, **22**, 15864–15873.

133 M. K. Taylor, T. Runčevski, J. Oktawiec, M. I. Gonzalez, R. L. Siegelman, J. A. Mason, J. Ye, C. M. Brown and J. R. Long, *J. Am. Chem. Soc.*, 2016, **138**, 15019–15026.

134 D. Banerjee, H. Wang, A. M. Plonka, T. J. Emge, J. B. Parise and J. Li, *Chem.–Eur. J.*, 2016, **22**, 11816–11825.

135 X. Sun, S. Yao, G. Li, L. Zhang, Q. Huo and Y. Liu, *Inorg. Chem.*, 2017, **56**, 6645–6651.

136 E. R. Engel, A. Jouaiti, C. X. Bezuidenhout, M. W. Hosseini and L. J. Barbour, *Angew. Chem.*, 2017, **129**, 9000–9004.

137 P. Lama and L. J. Barbour, *J. Am. Chem. Soc.*, 2018, **140**, 2145–2150.

138 S. Sen, N. Hosono, J.-J. Zheng, S. Kusaka, R. Matsuda, S. Sakaki and S. Kitagawa, *J. Am. Chem. Soc.*, 2017, **139**, 18313–18321.

139 S. Krause, V. Bon, U. Stoeck, I. Senkovska, D. M. Toebbens, D. Wallacher and S. Kaskel, *Angew. Chem., Int. Ed.*, 2017, **56**, 10676–10680.

140 S. Krause, V. Bon, H. Du, R. E. Dunin-Borkowski, U. Stoeck, I. Senkovska and S. Kaskel, *Beilstein J. Nanotechnol.*, 2019, **10**, 1737–1744.

141 J. Jin, X. Zhao, P. Feng and X. Bu, *Angew. Chem., Int. Ed.*, 2018, **57**, 3737–3741.

142 H. Yang, F. Guo, P. Lama, W.-Y. Gao, H. Wu, L. J. Barbour, W. Zhou, J. Zhang, B. Aguila and S. Ma, *ACS Cent. Sci.*, 2018, **4**, 1194–1200.

143 Y.-X. Shi, W.-X. Li, W.-H. Zhang and J.-P. Lang, *Inorg. Chem.*, 2018, **57**, 8627–8633.

144 S.-Q. Wang, Q.-Y. Yang, S. Mukherjee, D. O’Nolan, E. Patyk-Kazmierczak, K.-J. Chen, M. Shivanna, C. Murray, C. C. Tang and M. J. Zaworotko, *Chem. Commun.*, 2018, **54**, 7042–7045.

145 S.-Q. Wang, S. Mukherjee, E. Patyk-Kazmierczak, S. Darwish, A. Bajpai, Q.-Y. Yang and M. J. Zaworotko, *Angew. Chem., Int. Ed.*, 2019, **58**, 6630–6634.

146 A.-X. Zhu, Q.-Y. Yang, A. Kumar, C. Crowley, S. Mukherjee, K.-J. Chen, S.-Q. Wang, D. O’Nolan, M. Shivanna and M. J. Zaworotko, *J. Am. Chem. Soc.*, 2018, **140**, 15572–15576.

147 A.-X. Zhu, Q.-Y. Yang, S. Mukherjee, A. Kumar, C.-H. Deng, A. A. Bezrukov, M. Shivanna and M. J. Zaworotko, *Angew. Chem., Int. Ed.*, 2019, **58**, 18212–18217.

148 X. Wang, R. Krishna, L. Li, B. Wang, T. He, Y.-Z. Zhang, J.-R. Li and J. Li, *Chem. Eng. J.*, 2018, **346**, 489–496.

149 A. Hazra, D. P. van Heerden, S. Sanyal, P. Lama, C. Esterhuysen and L. J. Barbour, *Chem. Sci.*, 2019, **10**, 10018–10024.

150 S. Millan, B. Gil-Hernandez, E. Milles, S. Gokpinar, G. Makhloufi, A. Schmitz, C. Schlusener and C. Janiak, *Dalton Trans.*, 2019, **48**, 8057–8067.

151 B.-Q. Song, Q.-Y. Yang, S.-Q. Wang, M. Vandichel, A. Kumar, C. Crowley, N. Kumar, C.-H. Deng, V. Gascon Perez, M. Lusi, H. Wu, W. Zhou and M. J. Zaworotko, *J. Am. Chem. Soc.*, 2020, **142**, 6896–6901.

152 Q. Dong, X. Zhang, S. Liu, R. B. Lin, Y. Guo, Y. Ma, A. Yonezu, R. Krishna, G. Liu, J. Duan, R. Matsuda, W. Jin and B. Chen, *Angew. Chem., Int. Ed.*, 2020, **59**, 22756–22762.

153 A. Kondo, H. Kajiro, T. Nakagawa, H. Tanaka and H. Kanoh, *Dalton Trans.*, 2020, **49**, 3692–3699.

154 K. Roztocki, F. Formalik, A. Krawczuk, I. Senkovska, B. Kuchta, S. Kaskel and D. Matoga, *Angew. Chem., Int. Ed.*, 2020, **59**, 4491–4497.

155 F. Millange and R. I. Walton, *Isr. J. Chem.*, 2018, **58**, 1019–1035.



156 F. Millange, C. Serre and G. Ferey, *Chem. Commun.*, 2002, 822–823.

157 G. Ferey, M. Latroche, C. Serre, F. Millange, T. Loiseau and A. Percheron-Guegan, *Chem. Commun.*, 2003, 2976–2977.

158 T. R. Whitfield, X. Wang, L. Liu and A. J. Jacobson, *Solid State Sci.*, 2005, **7**, 1096–1103.

159 E. V. Anokhina, M. Vougo-Zanda, X. Wang and A. J. Jacobson, *J. Am. Chem. Soc.*, 2005, **127**, 15000–15001.

160 M. Vougo-Zanda, J. Huang, E. Anokhina, X. Wang and A. J. Jacobson, *Inorg. Chem.*, 2008, **47**, 11535–11542.

161 J. P. S. Mowat, S. R. Miller, A. M. Z. Slawin, V. R. Seymour, S. E. Ashbrook and P. A. Wright, *Microporous Mesoporous Mater.*, 2011, **142**, 322–333.

162 N. L. Rosi, J. Kim, M. Eddaoudi, B. Chen, M. O'Keeffe and O. M. Yaghi, *J. Am. Chem. Soc.*, 2005, **127**, 1504–1518.

163 A. Schoedel, M. Li, D. Li, M. O'Keeffe and O. M. Yaghi, *Chem. Rev.*, 2016, **116**, 12466–12535.

164 D. J. O'Hearn, A. Bajpai and M. J. Zaworotko, *Small*, 2021, **17**, 2006351.

165 C. Serre, F. Millange, C. Thouvenot, M. Nogues, G. Marsolier, D. Louër and G. Férey, *J. Am. Chem. Soc.*, 2002, **124**, 13519–13526.

166 T. Loiseau, C. Serre, C. Huguenard, G. Fink, F. Taulelle, M. Henry, T. Bataille and G. Férey, *Chem.-Eur. J.*, 2004, **10**, 1373–1382.

167 N. Guillou, F. Millange and R. I. Walton, *Chem. Commun.*, 2011, **47**, 713–715.

168 C. Serre, S. Bourrelly, A. Vimont, N. A. Ramsahye, G. Maurin, P. L. Llewellyn, M. Daturi, Y. Filinchuk, O. Leynaud, P. Barnes and G. Ferey, *Adv. Mater.*, 2007, **19**, 2246–2251.

169 S. Bourrelly, B. Moulin, A. Rivera, G. Maurin, S. Devautour-Vinot, C. Serre, T. Devic, P. Horcajada, A. Vimont, G. Clet, M. Daturi, J.-C. Lavalle, S. Loera-Serna, R. Denoyel, P. L. Llewellyn and G. Ferey, *J. Am. Chem. Soc.*, 2010, **132**, 9488–9498.

170 T. K. Trung, P. Trens, N. Tanchoux, S. Bourrelly, P. L. Llewellyn, S. Loera-Serna, C. Serre, T. Loiseau, F. Fajula and G. Ferey, *J. Am. Chem. Soc.*, 2008, **130**, 16926–16932.

171 V. Finsy, C. E. A. Kirschhock, G. Vedts, M. Maes, L. Alaerts, D. E. De Vos, G. V. Baron and J. F. M. Denayer, *Chem.-Eur. J.*, 2009, **15**, 7724–7731.

172 F. Millange, N. Guillou, R. I. Walton, J.-M. Grenache, I. Margiolaki and G. Ferey, *Chem. Commun.*, 2008, 4732–4734.

173 F. Millange, C. Serre, N. Guillou, G. Ferey and R. I. Walton, *Angew. Chem., Int. Ed.*, 2008, **47**, 4100–4105.

174 P. Horcajada, C. Serre, G. Maurin, N. A. Ramsahye, F. Balas, M. Vallet-Regi, M. Sebbar, F. Taulelle and G. Ferey, *J. Am. Chem. Soc.*, 2008, **130**, 6774–6780.

175 F. Millange, N. Guillou, M. E. Medina, G. Ferey, A. Carlin-Sinclair, K. M. Golden and R. I. Walton, *Chem. Mater.*, 2010, **22**, 4237–4245.

176 R. I. Walton, A. S. Munn, N. Guillou and F. Millange, *Chem.-Eur. J.*, 2011, **17**, 7069–7079.

177 R. El Osta, A. Carlin-Sinclair, N. Guillou, R. I. Walton, F. Vermoortele, M. Maes, D. de Vos and F. Millange, *Chem. Mater.*, 2012, **24**, 2781–2791.

178 B. Van de Voorde, A. S. Munn, N. Guillou, F. Millange, D. E. De Vos and R. I. Walton, *Phys. Chem. Chem. Phys.*, 2013, **15**, 8606–8615.

179 M. Sanselme, J.-M. Grenèche, M. Riou-Cavellec and G. Férey, *Solid State Sci.*, 2004, **6**, 853–858.



180 S. Bauer, C. Serre, T. Devic, P. Horcajada, J. Marrot, G. Férey and N. Stock, *Inorg. Chem.*, 2008, **47**, 7568–7576.

181 T. Devic, P. Horcajada, C. Serre, F. Salles, G. Maurin, B. Moulin, D. Heurtaux, G. Clet, A. Vimont, J.-M. Grenache, B. Le Ouay, F. Moreau, E. Magnier, Y. Filinchuk, J. Marrot, J.-C. Lavalle, M. Daturi and G. Ferey, *J. Am. Chem. Soc.*, 2010, **132**, 1127–1136.

182 N. A. Ramsahye, T.-K. Trung, S. Bourrelly, Q.-Y. Yang, T. Devic, G. Maurin, P. Horcajada, P. L. Llewellyn, P. Yot, C. Serre, Y. Filinchuk, F. Fajula, G. Ferey and P. Trems, *J. Phys. Chem. C*, 2011, **115**, 18683–18695.

183 T. Devic, F. Salles, S. Bourrelly, B. Moulin, G. Maurin, P. Horcajada, C. Serre, A. Vimont, J.-C. Lavalle, H. Leclerc, G. Clet, M. Daturi, P. L. Llewellyn, Y. Filinchuk and G. Ferey, *J. Mater. Chem.*, 2012, **22**, 10266–10273.

184 K. Seki and W. Mori, *J. Phys. Chem. B*, 2002, **106**, 1380–1385.

185 R. Kitaura, F. Iwahori, R. Matsuda, S. Kitagawa, Y. Kubota, M. Takata and T. C. Kobayashi, *Inorg. Chem.*, 2004, **43**, 6522–6524.

186 H. Chun, D. N. Dybtsev, H. Kim and K. Kim, *Chem.-Eur. J.*, 2005, **11**, 3521–3529.

187 D. Tanaka, M. Higuchi, S. Horike, R. Matsuda, Y. Kinoshita, N. Yanai and S. Kitagawa, *Chem.-Asian J.*, 2008, **3**, 1343–1349.

188 F. Zarekarizi, M. Joharian and A. Morsali, *J. Mater. Chem. A*, 2018, **6**, 19288–19329.

189 D. N. Dybtsev, H. Chun and K. Kim, *Angew. Chem., Int. Ed.*, 2004, **43**, 5033–5036.

190 K. Uemura, Y. Yamasaki, Y. Komagawa, K. Tanaka and H. Kita, *Angew. Chem., Int. Ed.*, 2007, **46**, 6662–6665.

191 K. Uemura, Y. Yamasaki, F. Onishi, H. Kita and M. Ebihara, *Inorg. Chem.*, 2010, **49**, 10133–10143.

192 J. S. Grosch and F. Paesani, *J. Am. Chem. Soc.*, 2012, **134**, 4207–4215.

193 J. Y. Lee, L. Pan, X. Huang, T. J. Emge and J. Li, *Adv. Funct. Mater.*, 2011, **21**, 993–998.

194 H. Miura, V. Bon, I. Senkovska, S. Ehrling, S. Watanabe, M. Ohba and S. Kaskel, *Dalton Trans.*, 2017, **46**, 14002–14011.

195 M. Shivanna, Q.-Y. Yang, A. Bajpai, E. Patyk-Kazmierczak and M. J. Zaworotko, *Nat. Commun.*, 2018, **9**, 3080.

196 P. Nugent, Y. Belmabkhout, S. D. Burd, A. J. Cairns, R. Luebke, K. Forrest, T. Pham, S. Q. Ma, B. Space, L. Wojtas, M. Eddaoudi and M. J. Zaworotko, *Nature*, 2013, **495**, 80–84.

197 X. L. Cui, K. J. Chen, H. B. Xing, Q. W. Yang, R. Krishna, Z. B. Bao, H. Wu, W. Zhou, X. L. Dong, Y. Han, B. Li, Q. L. Ren, M. J. Zaworotko and B. L. Chen, *Science*, 2016, **353**, 141–144.

198 S. K. Elsaidi, M. H. Mohamed, C. M. Simon, E. Braun, T. Pham, K. A. Forrest, W. Xu, D. Banerjee, B. Space, M. J. Zaworotko and P. K. Thallapally, *Chem. Sci.*, 2017, **8**, 2373–2380.

199 L. Yang, X. Cui, Y. Zhang, Q. Yang and H. Xing, *J. Mater. Chem. A*, 2018, **6**, 24452–24458.

200 L. Carlucci, G. Ciani, D. M. Proserpio and A. Sironi, *J. Chem. Soc., Chem. Commun.*, 1994, 2755–2756.

201 M. J. Zaworotko, *Chem. Soc. Rev.*, 1994, **23**, 283–288.

202 S. K. Elsaidi, M. H. Mohamed, L. Wojtas, A. Chanthapally, T. Pham, B. Space, J. J. Vittal and M. J. Zaworotko, *J. Am. Chem. Soc.*, 2014, **136**, 5072–5077.

203 E. J. Carrington, C. A. McAnally, A. J. Fletcher, S. P. Thompson, M. Warren and L. Brammer, *Nat. Chem.*, 2017, **9**, 882–889.

204 S. Galli, N. Masciocchi, V. Colombo, A. Maspero, G. Palmisano, F. J. López-Garzón, M. Domingo-García, I. Fernández-Morales, E. Barea and J. A. R. Navarro, *Chem. Mater.*, 2010, **22**, 1664–1672.

205 T. G. Mitina and V. A. Blatov, *Cryst. Growth Des.*, 2013, **13**, 1655–1664.

206 M. J. Zaworotko, *Chem. Commun.*, 2001, 1–9.

207 M. Fujita, Y. J. Kwon, S. Washizu and K. Ogura, *J. Am. Chem. Soc.*, 1994, **116**, 1151–1152.

208 J. Lu, T. Paliwala, S. C. Lim, C. Yu, T. Niu and A. J. Jacobson, *Inorg. Chem.*, 1997, **36**, 923–929.

209 K. Biradha, A. Mondal, B. Moulton and M. J. Zaworotko, *J. Chem. Soc., Dalton Trans.*, 2000, 3837–3844.

210 J. vanden Bergh, C. Güçüyener, E. A. Pidko, E. J. M. Hensen, J. Gascon and F. Kapteijn, *Chem.-Eur. J.*, 2011, **17**, 8832–8840.

211 D. Fairen-Jimenez, S. A. Moggach, M. T. Wharmby, P. A. Wright, S. Parsons and T. Düren, *J. Am. Chem. Soc.*, 2011, **133**, 8900–8902.

212 N. Lock, Y. Wu, M. Christensen, L. J. Cameron, V. K. Peterson, A. J. Bridgeman, C. J. Kepert and B. B. Iversen, *J. Phys. Chem. C*, 2010, **114**, 16181–16186.

213 L. Sarkisov, R. L. Martin, M. Haranczyk and B. Smit, *J. Am. Chem. Soc.*, 2014, **136**, 2228–2231.

214 S. Bourrelly, P. L. Llewellyn, C. Serre, F. Millange, T. Loiseau and G. Férey, *J. Am. Chem. Soc.*, 2005, **127**, 13519–13521.

215 N. Rosenbach Jr, A. Ghoufi, I. Deroche, P. L. Llewellyn, T. Devic, S. Bourrelly, C. Serre, G. Ferey and G. Maurin, *Phys. Chem. Chem. Phys.*, 2010, **12**, 6428–6437.

216 R. Demuynck, S. M. J. Rogge, L. Vanduyfhuys, J. Wieme, M. Waroquier and V. Van Speybroeck, *J. Chem. Theory Comput.*, 2017, **13**, 5861–5873.

217 R. Numaguchi, H. Tanaka, S. Watanabe and M. T. Miyahara, *J. Chem. Phys.*, 2013, **138**, 054708.

218 M. Pera-Titus and D. Farrusseng, *J. Phys. Chem. C*, 2012, **116**, 1638–1649.

219 A. Gonzalez-Nelson, F.-X. Coudert and M. A. van der Veen, *Nanomaterials*, 2019, **9**, 330.

220 M. P. Suh, H. J. Park, T. K. Prasad and D.-W. Lim, *Chem. Rev.*, 2012, **112**, 782–835.

221 L. J. Murray, M. Dinca and J. R. Long, *Chem. Soc. Rev.*, 2009, **38**, 1294–1314.

222 B. Li, H.-M. Wen, W. Zhou, J. Q. Xu and B. Chen, *Chem.*, 2016, **1**, 557–580.

223 K. Sumida, D. L. Rogow, J. A. Mason, T. M. McDonald, E. D. Bloch, Z. R. Herm, T.-H. Bae and J. R. Long, *Chem. Rev.*, 2012, **112**, 724–781.

224 S. Kitagawa, *Angew. Chem., Int. Ed.*, 2015, **54**, 10686–10687.

225 M. Bonneau, C. Lavenn, K. Sugimoto, A. Legrand, T. Ogawa, F.-X. Coudert, R. Réau, K.-i. Otake and S. Kitagawa, *Research Square*, 2020, DOI: 10.21203/rs.3.rs-102861/v1.

226 Y. Peng, V. Krungleviciute, I. Eryazici, J. T. Hupp, O. K. Farha and T. Yildirim, *J. Am. Chem. Soc.*, 2013, **135**, 11887–11894.

227 F. G  ndara, H. Furukawa, S. Lee and O. M. Yaghi, *J. Am. Chem. Soc.*, 2014, **136**, 5271–5274.

228 B. Li, H.-M. Wen, H. Wang, H. Wu, M. Tyagi, T. Yildirim, W. Zhou and B. Chen, *J. Am. Chem. Soc.*, 2014, **136**, 6207–6210.

229 J. A. Mason, M. Veenstra and J. R. Long, *Chem. Sci.*, 2014, **5**, 32–51.

230 D. Alezi, Y. Belmabkhout, M. Suyetin, P. M. Bhatt, L. J. Weseli  ski, V. Solovyeva, K. Adil, I. Spanopoulos, P. N. Trikalitis and A.-H. Emwas, *J. Am. Chem. Soc.*, 2015, **137**, 13308–13318.

231 J. M. Lin, C. T. He, Y. Liu, P. Q. Liao, D. D. Zhou, J. P. Zhang and X. M. Chen, *Angew. Chem., Int. Ed.*, 2016, **55**, 4674–4678.

232 I. Spanopoulos, C. Tsangarakis, E. Klontzas, E. Tylianakis, G. Froudakis, K. Adil, Y. Belmabkhout, M. Eddaoudi and P. N. Trikalitis, *J. Am. Chem. Soc.*, 2016, **138**, 1568–1574.

233 Z. Chen, P. Li, R. Anderson, X. Wang, X. Zhang, L. Robison, L. R. Redfern, S. Moribe, T. Islamoglu, D. A. G  mez-Gualdr  n, T. Yildirim, J. F. Stoddart and O. K. Farha, *Science*, 2020, **368**, 297–303.

234 Y. He, W. Zhou and B. Chen, Current status of porous metal–organic frameworks for methane storage, *Metal–Organic Frameworks: Applications in Separations and Catalysis*, Wiley-VCH, 2018, pp. 163–198.

235 Z. R. Herm, E. D. Bloch and J. R. Long, *Chem. Mater.*, 2014, **26**, 323–338.

236 B. Li, H. Wang and B. Chen, *Chem.-Asian J.*, 2014, **9**, 1474–1498.

237 B. Van de Voorde, B. Bueken, J. Denayer and D. De Vos, *Chem. Soc. Rev.*, 2014, **43**, 5766–5788.

238 K. Adil, Y. Belmabkhout, R. S. Pillai, A. Cadiou, P. M. Bhatt, A. H. Assen, G. Maurin and M. Eddaoudi, *Chem. Soc. Rev.*, 2017, **46**, 3402–3430.

239 S. Mukherjee, A. V. Desai and S. K. Ghosh, *Coord. Chem. Rev.*, 2018, **367**, 82–126.

240 H. Wang and J. Li, *Acc. Chem. Res.*, 2019, **52**, 1968–1978.

241 R.-B. Lin, S. Xiang, W. Zhou and B. Chen, *Chem.*, 2020, **6**, 337–363.

242 D. S. Sholl and R. P. Lively, *Nature*, 2016, **532**, 435–437.

243 L. Li, Y. Wang, J. Yang, X. Wang and J. Li, *J. Mater. Chem. A*, 2015, **3**, 22574–22583.

244 L. Alaerts, M. Maes, L. Giebel, P. A. Jacobs, J. A. Martens, J. F. M. Denayer, C. E. A. Kirschhock and D. E. De Vos, *J. Am. Chem. Soc.*, 2008, **130**, 14170–14178.

245 V. Finsy, C. E. A. Kirschhock, G. Vedts, M. Maes, L. Alaerts, D. E. De Vos, G. V. Baron and J. F. M. Denayer, *Chem.-Eur. J.*, 2009, **15**, 7724–7731.

246 V. Bon, N. Kavoosi, I. Senkovska and S. Kaskel, *ACS Appl. Mater. Interfaces*, 2015, **7**, 22292–22300.

247 J.-P. Zhang, P.-Q. Liao, H.-L. Zhou, R.-B. Lin and X.-M. Chen, *Chem. Soc. Rev.*, 2014, **43**, 5789–5814.

248 J. D. Evans, V. Bon, I. Senkovska, H.-C. Lee and S. Kaskel, *Nat. Commun.*, 2020, **11**, 2690.

249 T. D. Bennett, A. K. Cheetham, A. H. Fuchs and F.-X. Coudert, *Nat. Chem.*, 2017, **9**, 11–16.

250 X. Yang, H.-L. Zhou, C.-T. He, Z.-W. Mo, J.-W. Ye, X.-M. Chen and J.-P. Zhang, *Research*, 2019, **2019**, 9463719.

251 S. Ehrling, E. M. Reynolds, V. Bon, I. Senkovska, T. E. Gorelik, J. D. Evans, M. Rauche, M. Mendt, M. S. Weiss, A. Pöppl, E. Brunner, U. Kaiser, A. L. Goodwin and S. Kaskel, *Nat. Chem.*, 2021, **13**, 568–574.

252 S. Chibani and F.-X. Coudert, *APL Mater.*, 2020, **8**, 080701.

253 G. Fraux and F.-X. Coudert, *Chem. Commun.*, 2017, **53**, 7211–7221.

254 F.-X. Coudert, *Phys. Chem. Chem. Phys.*, 2010, **12**, 10904–10913.

255 F. J. Sotomayor and C. M. Lastoskie, *Microporous Mesoporous Mater.*, 2020, **292**, 109371.

256 S. Darwish, S.-Q. Wang, D. M. Croker, G. M. Walker and M. J. Zaworotko, *ACS Sustainable Chem. Eng.*, 2019, **7**, 19505–19512.

257 N. Stock and S. Biswas, *Chem. Rev.*, 2012, **112**, 933–969.

258 N. Chanut, A. Ghoufi, M.-V. Coulet, S. Bourrelly, B. Kuchta, G. Maurin and P. L. Llewellyn, *Nat. Commun.*, 2020, **11**, 1216.

259 J. Su, S. Yuan, H.-Y. Wang, L. Huang, J.-Y. Ge, E. Joseph, J. Qin, T. Cagin, J.-L. Zuo and H.-C. Zhou, *Nat. Commun.*, 2017, **8**, 1–8.

260 H. Li and M. R. Hill, *Acc. Chem. Res.*, 2017, **50**, 778–786.

261 C. Jones, A. Tansell and T. Easun, *J. Mater. Chem. A*, 2016, **4**, 6714–6723.

